Pathological expansion of gut microbiome-associated *Enterococcus* in advanced cirrhosis corresponds with multilevel perturbations of the gut-liver-immune axis

Authors

Matthew J Dalby[1,2], Raymond Kiu[1,2], Marilena Stamouli[3], Betsy Arefaine[3], Lex E X Leong[4], Jack Hales[5], Christine Bernsmeier[6,7], Arjuna Singanayagam[8], Sidsel Støy[9], Maria-Emanuela Maxan[3,6], Merianne Mohamad[3], Ane Zamalloa[6], Matt Lewis[10], Royce P. Vincent[11,12], I. Jane Cox[3], Adrien Le Guennec[13], Roger Williams[18], Lindsey A Edwards[6], Shilpa Chokshi[3,14], Mark Thursz[10,15], Naiara Beraza[5], Charalambos G Antoniades[10], Geraint B Rogers[4], Julia A Wendon[3], Kenneth D Bruce[16], Debbie L Shawcross[3], Mark JW McPhail[3,6,10], *Lindsay J Hall[1,2,5,17], *Vishal C Patel[3,6]

Affiliations

1. Department of Microbes, Infection & Microbiomes, School of Infection, Inflammation and Immunology, College of Medicine & Health, University of Birmingham, Birmingham, UK.
2. Institute of Microbiology & Infection, University of Birmingham, Birmingham, UK.
3. Roger Williams Institute of Liver Studies, School of Immunology & Microbial Sciences, Faculty of Life Sciences and Medicine, King's College London, Foundation for Liver Research and King's College Hospital, London, UK
4. Infection & Immunity Theme, South Australian Health & Medical Research Institute, North Terrace, Adelaide, SA, Australia.
5. Food, Microbiome and Health, Quadram Institute Bioscience, Norwich Research Park, Norwich, UK.
6. Institute of Liver Studies, King's College Hospital NHS Foundation Trust, London, United Kingdom
7. Department of Biomedicine, University of Basel, Switzerland.
8. Infection Clinical Academic Group, St. George's School of Health and Medical Sciences, City St. George's University of London, Cranmer Terrace, London, SW17 0RE, UK.
9. Department of Hepatology and Gastroenterology, Aarhus University Hospital, DK-8200 Aarhus, Denmark.
10. Division of Digestive Disease, Department of Metabolism, Digestion & Reproduction, Imperial College London, London, UK.
11. Department of Clinical Biochemistry, King's College Hospital NHS Foundation Trust, London, UK;
12. Department of Nutritional Sciences, Faculty of Life Sciences and Medicine, King's College London, London, UK
13. Randall Centre for Cell & Molecular Biophysics and Centre for Biomolecular Spectroscopy, King's College London, London SE1 1UL, UK
14. Faculty of Health, University of Plymouth, Devon, UK

15. Imperial College Healthcare NHS Trust, St Mary's Hospital, Praed St, London, UK.
16. Institute of Pharmaceutical Science, King's College London, UK.
17. Norwich Medical School, University of East Anglia, Norwich Research Park, Norwich, UK.
18. In memoriam.
* Joint last and corresponding authors.

Keywords: cirrhosis; advanced chronic liver disease; acute-on-chronic liver failure; microbiota; microbiome; *Enterococcus*; bile acids, bacterial translocation, gut inflammation, systemic inflammation, monocyte dysfunction

Funding statement: The observational study was adopted to the National Institute for Health Research (NIHR) Clinical Research Network (CRN) portfolio, supporting participant screening and recruitment by the Liver Research and Anaesthetics, Critical Care, Emergency and Trauma Teams at King's College Hospital NHS Foundation Trust. VCP was supported by a New Investigator Award from the Intensive Care Foundation (Registered charity number: 2940178) and Clinical Research Network South London Principal Investigator Strategic "GreenShoot" Research Delivery and Development Funding. The clinical trial was funded through an investigator-initiated study grant awarded by Norgine Pharmaceuticals UK Limited to King's College London. Infrastructure to support the trial was also provided by the Medical Research Council (MRC) Centre for Transplantation, King's College London, UK – MRC grant no. MR/J006742/1. Laboratory assays were also part funded by a generous donation from a Liver Service User to the King's College Hospital Institute of Liver Studies and Transplantation Charity Research Fund, King's College Hospital Charity (Registered charity number: 1165593). MS, BA, MEM, MM, IJC, SC and VCP were supported and bioinformatic analyses were part funded by the Foundation for Liver Research (Registered charity number: 268211/1134579). LJH is supported by Wellcome Trust Investigator Award (220876/Z/20/Z); the Biotechnology and Biological Sciences Research Council (BBSRC), Institute Strategic Programme Gut Microbes and Health (BB/R012490/1), and its constituent projects BBS/E/F/000PR10353 and BBS/E/F/000PR10356, and the BBSRC Institute Strategic Programme Food, Microbiome and Health BB/X011054/1 and its constituent project BBS/E/QU/230001B. MT Acknowledges support from the NIHR-Imperial Biomedical Research Centre and the Medical Research Council Precision Medicine Award (MR/R014019/1).

Conflicts of interest:

DLS has undertaken consultancy for Norgine Pharmaceuticals Ltd, EnteroBiotix, MRM Health, Apollo Therapeutics, Genfit and Satellite Biosciences.

RPV reports Honoraria from Novo Nordisk, Amarin UK and AstraZeneca.

AS has delivered paid lectures for Bristol Myers Squibb.

VCP has undertaken consultancy for Norgine Pharmaceuticals Ltd, Alfasigma S.p.A. and Menarini Diagnostics Ltd.

MD, LH, RK, IJC, ALG, GR, SS, SC, KB, MJWM have no conflicts.

Authors contributions:

- Matthew J Dalby: Data curation, Formal analysis, Investigation, Software, Visualisation, Writing - Original Draft, Writing - Review & Editing
- Raymond Kiu: Data curation, Formal analysis, Writing - Review & Editing
- Marilena Stamouli: Data curation, Formal analysis, Writing - Review & Editing
- Betsy Arefaine: Data curation, Formal analysis
- Lex E X Leong: Data curation, Formal analysis, Investigation, Visualization, Writing - Review & Editing
- Jack Hales: Methodology, Writing - Review & Editing
- Christine Bernsmeier: Data curation, Formal analysis, Visualization, Writing - Review & Editing
- Arjuna Singanayagam: Data curation, Formal analysis, Visualization, Writing - Review & Editing
- Sidsel Støy: Data curation, Formal analysis, Visualization, Writing - Review & Editing
- Maria-Emanuela Maxan: Data curation, Writing - Review & Editing
- Merianne Mohamad: Visualization, Writing - Review & Editing
- Matt Lewis: Investigation, Methodology, Writing - Review & Editing
- Royce P Vincent: Resources, Writing - Review & Editing
- Jane Cox: Data curation, Formal analysis, Investigation, Visualization, Writing - Review & Editing
- Adrien Le Guennec: Data curation, Visualization, Writing - Review & Editing
- Roger Williams: Supervision
- Lindsey A Edwards: Data curation, Formal analysis, Writing - Review & Editing
- Shilpa Chokshi: Supervision, Writing – review & editing

- Mark Thursz: Resources, Supervision, Writing – review & editing
- Naiara Beraza: Investigation, Resources, Writing - Review & Editing
- Charalambos G Antoniades: Supervision
- Geraint B Rogers: Conceptualisation, Data curation, Formal analysis, Investigation, Resources, Supervision, Visualization, Writing - Review & Editing
- Julia A Wendon: Conceptualisation, Supervision, Writing – review & editing
- Kenneth D Bruce: Conceptualisation, Supervision, Writing – review & editing
- Debbie L Shawcross: Conceptualisation, Funding acquisition, Project administration, Resources, Supervision, Writing – review & editing, served as Chief Investigator of RIFSYS Trial
- Mark JW McPhail: Conceptualisation, Formal analysis, Supervision, Writing - Review & Editing
- Vishal C Patel: Conceptualisation, Funding acquisition, Investigation, Methodology, Project administration, Resources, Supervision, Writing – review & editing, served as Chief Investigator of GLA study
- Lindsay J Hall: Conceptualisation, Funding acquisition, Investigation, Methodology, Project administration, Resources, Supervision, Writing – review & editing

Data availability:

The 16S rRNA amplicon sequencing raw reads are deposited in NCBI SRA under project PRJNA1223169.

Abstract

Background: Chronic liver disease (CLD) is a progressive condition that, in its advanced stages, leads to cirrhosis with related clinical complications, and can lead to acute-on-chronic liver failure (ACLF) - a syndrome marked by critical illness, multi-organ dysfunction and high mortality. Systemic inflammation in ACLF can occur without overt infection, indicating alternative pathways of immune activation and microbial translocation. Intestinal perturbations, bacterial translocation, and the resulting systemic inflammation and immune dysfunction are defining features of ACLF, yet the identification of specific microbial contributors remains poorly elucidated.

Objective: To investigate the relationship between gut microbiome alterations, systemic inflammation, and clinical markers of disease severity across the cirrhosis spectrum.

Design: This cross-sectional, prospective study analysed faecal microbiota, plasma bile acids, urinary and plasma metabolites, markers of gut and systemic inflammation and translocation, and monocyte dysfunction, in a well-phenotyped cohort of patients with ACLF, decompensated cirrhosis and stable cirrhosis, in comparison with healthy individuals.

Results: Advanced stages of cirrhosis were marked by a higher abundance of *Enterococcus*, which correlated with markers of systemic inflammation, particularly in ACLF patients. Concurrently, the abundance of anaerobic commensal genera such as *Roseburia*, *Ruminococcus*, and *Faecalibacterium* were significantly lower. Lower urinary hippurate and trimethylamine N-oxide TMAO levels, linked to reduced microbial metabolism and dietary fibre intake, paralleled these microbiome changes. While elevated plasma primary bile acids reflected hepatic dysfunction, systemic inflammatory markers suggested parallel gut barrier dysfunction and microbial translocation in advanced cirrhosis.

Conclusion: This study underscores a potential role of greater intestinal *Enterococcus* abundance, as cirrhosis severity increases and where clinically there is more antibiotic exposure, as a driver of gut barrier inflammation and dysfunction, and systemic immune dysfunction in advanced cirrhosis. Further research into tailored microbiome-targeted therapies, including prebiotics and probiotics, and more focused antibiotic use may prevent *Enterococcus* dominance and restore gut-liver axis homeostasis and mitigate disease progression in CLD.

Key messages

What is already known on this topic:

- CLD can progress to ACLF, a life-threatening syndrome with high mortality rates characterised by systemic inflammation, impaired phagocytosis and immune dysfunction with associated multiple organ failure.
- The gut microbiome's role in underpinning the gut-liver axis is recognised, with microbial perturbations and gut barrier dysfunction associated with CLD, yet the exact microbiome changes and their link to inflammatory pathways remain unclear.

What this study adds:

- This study reveals that *Enterococcus* significantly increases with CLD severity and antibiotic use and correlates with markers of systemic inflammation and gut barrier dysfunction.
- Reductions in obligate anaerobe commensal bacteria, such as *Roseburia* and *Faecalibacterium*, are observed, alongside depressed levels of key microbial metabolites, including hippurate and TMAO, across CLD stages.
- These changes suggest that *Enterococcus* predominance and gut microbiome perturbations driven by factors including disease severity and antibiotic use may actively drive inflammation and impaired monocyte function in CLD.

How this study might affect research, practice, or policy:

- Findings indicate that *Enterococcus* and wider gut microbiome perturbations provide a rationale for targeting as therapeutic strategies to modulate the gut-liver axis in CLD.
- This highlights the potential of microbiome-focused interventions, such as faecal microbial transplantation, probiotics, prebiotics or phages, to improve gut health, reduce gut and systemic inflammation, and ultimately mitigate cirrhosis-related complications.
- Future research and development of targeted microbiome therapeutics may positively influence CLD management including a focus on antimicrobial stewardship, and inform clinical guidelines whilst improving patient outcomes.

1. Introduction

Chronic liver disease (CLD) is a progressive condition, resulting from several different aetiologies such as alcohol, viral hepatitis, and obesity that can culminate in cirrhosis and eventual liver failure (Huang et al., 2023). An important aspect of CLD is the development of acute-on-chronic liver failure (ACLF), a distinct syndrome characterised by multi-organ dysfunction, worsening liver function, and liver failure, with high mortality rates (Katoonizadeh et al., 2010; Moreau et al., 2013; Shah et al., 2024). The transition to decompensated cirrhosis, preceding ACLF, can lack identifiable triggers, confounding therapeutic options, exacerbating morbidity, and reducing transplant-free survival (D'Amico et al., 2022; Trebicka et al., 2021).

The gut microbiota is a key component of the 'gut-liver axis' but its interplay with the disease mechanisms is still not fully understood in CLD (Albillos et al., 2020; Hsu and Schnabl, 2023). While bacterial infections can act as a trigger of progression to ACLF, many cases (60-70%) display systemic inflammation without identifiable infection, with 50% of patients with 'sepsis' culture negative, suggesting alternative inflammatory pathways and limitations in infection diagnosis methods (Hernaez et al., 2017; Toledo et al., 1993). This 'sterile inflammation' in CLD patients may be driven by damage-associated molecular patterns (DAMPs) released from stressed or dying hepatocytes particularly in those without clear triggers such as active alcohol use or culture-confirmed bacterial infections (Arroyo et al., 2015). Additionally, translocation of viable bacteria or microbial components (i.e. microbial-associated molecular patterns [MAMPs]) via a dysfunctional intestinal barrier, may contribute to systemic inflammation, precipitating cirrhosis-related complications. Increased markers of gut permeability and inflammation in CLD patients further support the link between microbial translocation and inflammatory responses (Alexopoulou et al., 2017).

The gut microbiota potentially plays a dual role in CLD, serving as a reservoir for pathogens and MAMPs, while also simultaneously maintaining gut homeostasis through its resident commensal bacteria (Adak and Khan, 2019; Caballero-Flores et al., 2023). These commensal microbes are critical for gut epithelial integrity, pathobiont exclusion (and preventing overgrowth), and metabolite production (e.g. short-chain fatty acids [SCFAs]) essential for host health (Ghosh et al., 2021). In CLD, however, gut microbiota disruptions are frequently observed, associated with reduced intestinal

194 barrier integrity, leading to increased microbial translocation. This process introduces intestinal
195 bacteria and MAMPs into the systemic circulation, contributing to cirrhosis-related inflammation,
196 particularly in advanced disease stages. Studies in CLD have reported reductions in commensal
197 bacterial genera such as *Ruminococcus, Faecalibacterium, Bacteroidetes,* and *Coprococcus* (Da Silva
198 et al., 2018; Dubinkina et al., 2017), accompanied by increases in pathobiont taxa like
199 *Enterococcaceae*, *Staphylococcaceae*, and *Enterobacteriaceae* (Bajaj et al., 2014). Additionally,
200 patients with CLD show altered bile acid homeostasis, characterised by alterations in bile acid
201 quantities and composition, which correlate with microbiota shifts and reduced conversion of
202 primary to secondary bile acids (Kakiyama et al., 2013; Mouzaki et al., 2016), with more primary bile
203 acids being found in faeces (Kakiyama et al., 2014). These changes, mirrored in serum bile acids,
204 worsen with cirrhosis progression (Horvatits et al., 2017). However, comprehensive studies
205 integrating microbiota alterations to systemic metabolites, inflammatory and gut barrier markers,
206 across CLD stages remain limited. (Bajaj et al., 2022, 2014, 2012).

207 This study aimed to identify alterations in bacterial genera in the faecal microbiota, as targets for
208 future therapeutic intervention, across a well-phenotyped cohort of patients with ACLF,
209 decompensated cirrhosis, stable cirrhosis, and healthy controls. We aimed to understand some of
210 the potential functional properties in these microbiome changes by comparison with profiling of
211 serum bile acids, urinary and plasma metabolites, and markers of gut inflammation, bacterial
212 translocation and systemic immune activation, as key pathobiological processes within the gut-liver-
213 immune axis. We hypothesised that microbiota perturbations increase with CLD severity. By
214 correlating these microbiota differences with relevant metabolic, inflammatory, immunological and
215 clinical disease markers, we aimed to detect key target bacteria within the gut that are associated
216 with disruption within the gut-liver-immune axis, providing insights into disease pathobiology and
217 informing potential therapeutic targets.

2. Results

2.1 Participant characteristics

This cross-sectional cohort included patients with cirrhosis who were categorised based on disease stage and severity; stable cirrhosis (SC), decompensated cirrhosis (DC), or acute-on-chronic liver failure (ACLF). A healthy control (HC) group of healthy participants was included for comparison analysis and to establish normal values. Table 1 summarises demographic, clinical and biochemical characteristics of the recruited patients and healthy controls. A total of 153 patients with cirrhosis were included in this study (SC=15, DC=81, ACLF=57) with 40 HCs. Patients with cirrhosis were older than HC with a mean HC age of 38 years (SD: 10 years) and mean liver cohort age of 53 years (SD: 11 years). Predominant aetiologies of cirrhosis included alcohol-related liver disease (ARLD) (SC/DC/ACLF: 60%/70.4%/57.9%) and metabolic- dysfunction associated steatotic liver disease (MASLD) (SC/DC/ACLF: 20%/8.6%/10.5%), respectively. SC, DC and ACLF patients presented with ascites (33.3%/71.6%/96.5%) and HE (6.7%/43.2%/86%) as predominant manifestations of hepatic decompensation, respectively. None of the cirrhosis patients had experienced a variceal haemorrhage in the 7 days prior to recruitment nor had spontaneous bacterial peritonitis at the time of sampling. DC and ACLF patients were more frequently receiving antibiotics acutely 45.7%/91.2%, respectively) compared to SC (20%). There was no difference in use of rifaximin-α (only five participants received rifaximin-α monotherapy as antibiotic treatment), lactulose, non-selective beta-blockers and acid suppression therapies (proton pump inhibitors, H2 antagonists) across the cirrhosis cohorts. Haematological, biochemical and disease severity and prognostic composite scores followed expected patterns. Transplant-free survival at 90 days was 77.8% and 24.6% for the DC and ACLF groups, respectively, with no deaths observed in the SC group.

2.2. Microbiota diversity, bacterial translocation, faecal calprotectin, serum bile acid, and metabolites profiles are progressively altered with increasing cirrhosis severity.

Initial analysis focused on the composition of the faecal microbiota, plasma bile acids, urinary metabolites and serum metabolites between cirrhosis severity groups in comparison to HCs. Faecal microbiota diversity, both the number of bacterial genera detected (**Figure 1A)** and the Inverse

245 Simpson diversity index (**Figure 1B**), was lower in patients with more advanced cirrhosis compared
246 to all other groups. Clustering analysis using non-metric multidimensional scaling (NMDS) shows
247 separation in gut microbiota composition between ACLF and HC, with DC clustered between HC and
248 ACLF, while SC clustered closely to HC (**Figure 1C; Supplementary File 2**). The overall effect of disease
249 severity was tested using a PERMANOVA test (R2 = 13.5%; P = 0.0001) and a pairwise comparison
250 showed that the ACLF group clustered separately ($P < 0.05$) from DC, SC, and HC groups with DC also
251 different to the HC group (**Supplementary File 6**). To assess the associations between clinical
252 metadata variables, NMDS analysis was specifically conducted on faecal sequencing data from
253 patients with cirrhosis excluding HCs. Envfit analysis was used to examine the influence of 69 clinical
254 variables on microbiota composition. Forty-one clinical variables were significantly associated with
255 microbiota composition in patients with cirrhosis, with measures of cirrhosis severity exhibiting the
256 most pronounced impact (**Supplementary Figure 1A; Supplementary File 7**). For the purposes of
257 visualisation the ten clinical variables with the highest R2 values with the strongest association with
258 the microbiota composition were overlaid on the NMDS plot and were all correlated with cirrhosis
259 severity (**Supplementary Figure 1B; Supplementary File 7**).

260 NMDS plots comparing plasma bile acid composition indicated higher divergence amongst HC
261 samples, and an increasing convergence (clustering) with cirrhosis severity (PERMANOVA: P=0.0001)
262 (**Figure 1D; Supplementary File 3,6**). Both urine (PERMANOVA: P=0.0001) and plasma metabolites
263 (PERMANOVA: P=0.0001) showed significant separation in clustering based on cirrhosis severity with
264 similar NMDS clustering with tightly clustered HC samples and divergent cirrhosis patient samples,
265 particularly for ACLF (**Figure 1E-F; Supplementary File 6**). Multivariate analysis, after obvious
266 exclusions including for dominant glucose or ethanol peaks, for example, showed separation of the
267 four study cohorts (HC, n=36; SC, n=8; DC, n=67; and ACLF, N=36) with pairwise multilevel comparison
268 showing significant differences between all groups except SC and DC ($P < 0.05$). This was also
269 confirmed visually by the NMDS plots (**Figure E; Supplementary File 5**) and relative metabolite levels
270 per grouping for TMAO, hippurate (**Figure 3F; Supplementary File 6**) and for creatinine, citrate,
271 dimethylamine, formate and mannitol (**Supplementary Figure 3**).

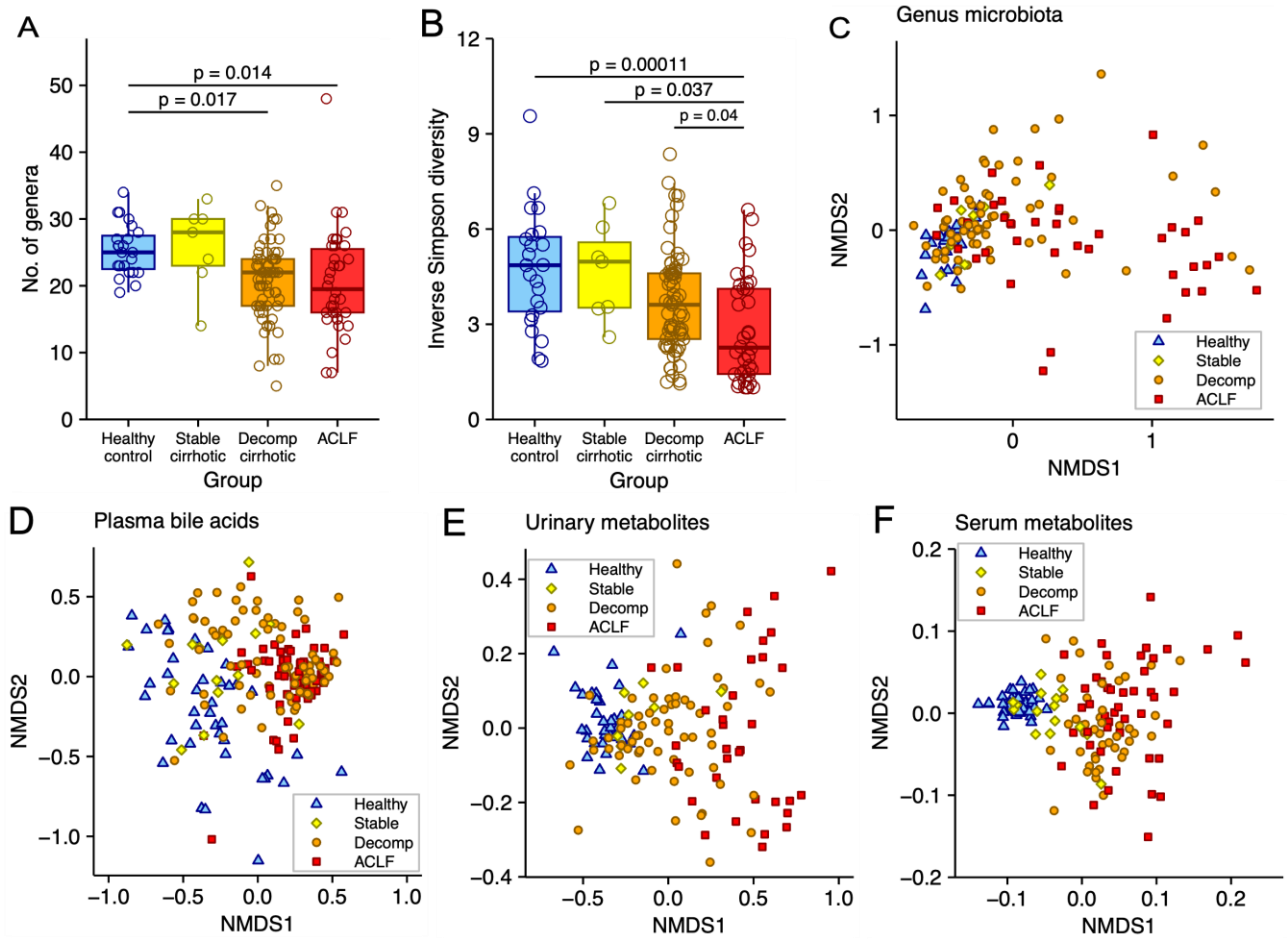

Figure 1: Comparison of faecal microbiota diversity, plasma bile acids, and metabolites profiles in cirrhosis and healthy controls.

(A) Number of genera detected in each participant's faecal sample by cirrhosis severity and HC. (B) Faecal microbiota diversity measured using the Inverse Simpson diversity index by cirrhosis severity vs HC. NMDS ordination shows dissimilarity indices via Bray-Curtis distances between individual participants coloured by cirrhosis severity vs HC (D) plasma bile acids (E) urinary metabolites and (F) serum metabolites. Dot and box plots show median and interquartile ranges of data with circles showing each individual participant.

2.3. Genus-level microbiota composition at different cirrhosis severities reveals a progressive overabundance of *Enterococcus* with reductions in commensal taxa.

283 To investigate alterations in gut microbiota composition in more detail, bacterial genus profiles
284 within individual participants were examined. Stacked bar plots showing the ten most abundant
285 bacterial genera illustrate an increasing dominance of *Enterococcus* in more advanced cirrhosis i.e.
286 DC and ACLF groups (**Figure 2A**). Differential abundance of bacterial genera is represented in a heat
287 map showing significant associations between faecal bacterial genera comparing the three cirrhosis
288 groups with HC (**Figure 2B; Supplementary file 8**). *Ruminococcus, Roseburia,* and *Lachnospira*
289 showed the strongest negative association with cirrhosis severity with the lowest abundances in ACLF
290 and DC patients compared to HC (**Figure 2C-E**). *Enterococcus* and *Staphylococcus* showed the
291 strongest positive association with cirrhosis severity with highest abundance in ACLF relative to HC
292 (**Figure 2FH**), while *Streptococcus* abundance was higher in DC and SC compared to HC (**Figure 2G)**.
293 *Enterococcus* abundance was markedly higher in the ACLF patient group compared to HC (**Figure 2C)**.
294 Conversely, a proportion of more severely ill patients with cirrhosis have gut microbiota dominated
295 by *Enterococcus*, with significantly elevated levels observed in DC and ACLF. In a quarter of ACLF
296 patients, the relative abundance of *Enterococcus* exceeded 75%.

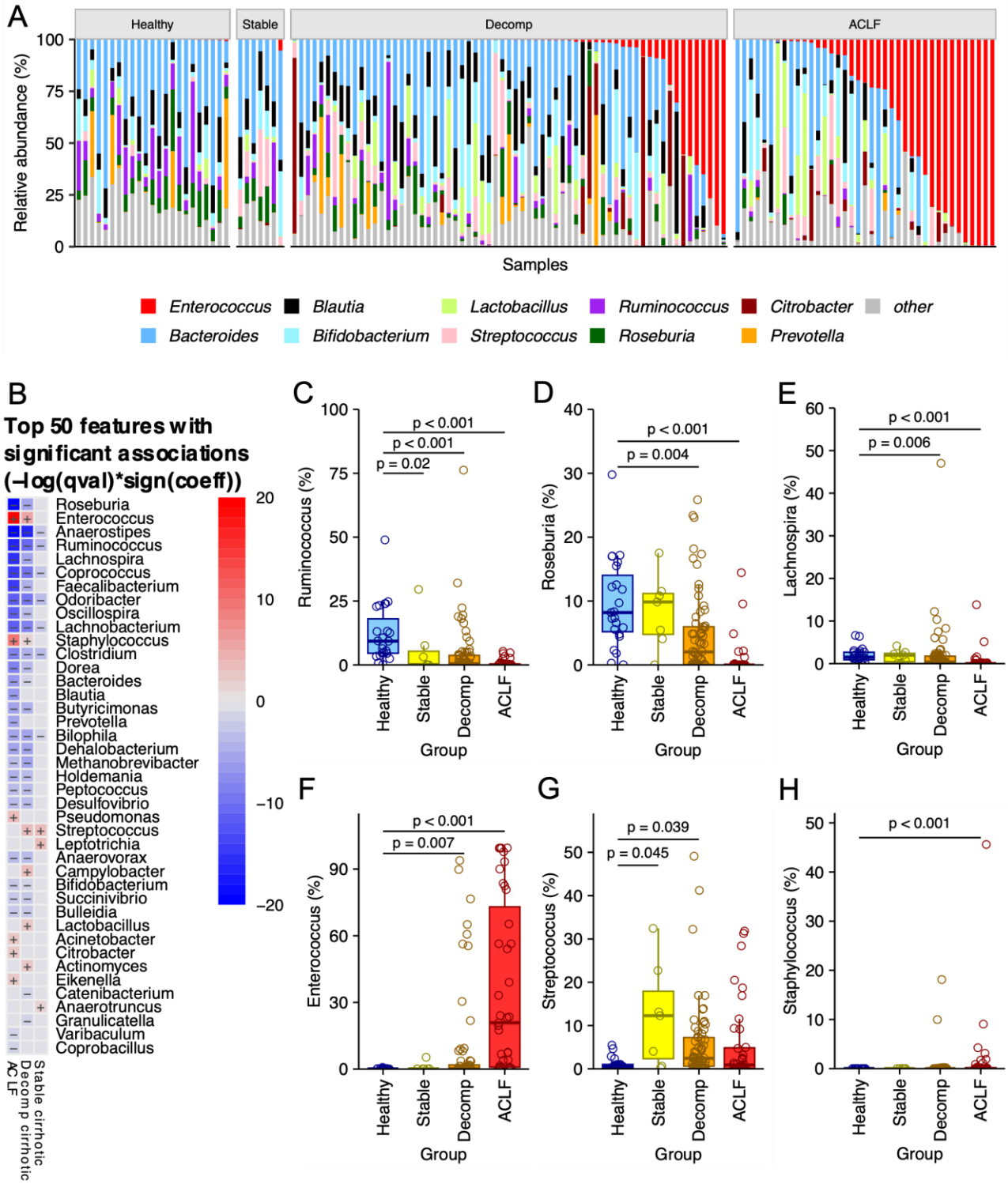

Figure 2: Microbiota genus composition in cirrhosis vs. healthy controls.

(A) Stacked bar plots show the ten most abundant bacterial genera in faecal samples stacked by overall abundance, and with participants ordered within cirrhosis severity categories by proportion

301 of *Enterococcus*. (B) The heat map displays MaAslin2 analysis of significant associations between
302 faecal genus abundance and cirrhosis severity with HC used as a reference. The three genera with
303 the strongest negative effect size for cirrhosis severity determined by MaAslin2 using HC as a
304 reference and shown as box and dot plots were (C) *Ruminococcus*, (D) *Roseburia*, and (E) *Lachnospira*.
305 The three genera with the strongest positive effect size for cirrhosis severity determined by MaAsLin2
306 using HC as a reference and shown as box and dot plots were (F) *Enterococcus*, (G) *Streptococcus*,
307 and (H) *Staphylococcus*. Dot and box plots show median and interquartile ranges of data with circles
308 showing each individual participant.

309 **2.4. Plasma bile acids and urinary metabolites correlate with specific gut microbiota taxa with**
310 **increasing cirrhosis severity.**

311 To determine the impact of cirrhosis severity on alterations in plasma bile acids, urinary metabolites,
312 and serum metabolites, we correlated these, using MaAsLin2, with faecal bacterial genera to
313 investigate their associations with gut microbiota composition and provide putative insights into
314 alterations in microbiome function. The primary bile acids taurochenodeoxycholic acid (TCDCA),
315 glycochenodeoxycholic acid (GCDCA), taurocholic acid (TCA) and glycocholic acid (GCA) were higher
316 in the plasma of patients with cirrhosis compared to HC, while other bile acids were lower than in HC
317 (**Figure 3A; Supplementary File 9**). TCDCA and GCDCA showed the strongest effect size with higher
318 concentrations in all three cirrhosis cohorts relative to HC (**Figure 3B-C; Supplementary Figure 3**).
319 Contrasting plasma bile acid concentrations with the percentage of bacterial genera showed that
320 *Enterococcus* abundance was positively correlated with primary bile acids including TCDCA, while
321 *Ruminococcus*, *Coprococcus*, and *Roseburia* were negatively correlated with primary bile acid
322 concentration (**Figure 3D; Supplementary Figure 2**).

323 Analysis of urinary metabolites showed several metabolites differing by cirrhosis severity relative to
324 HC (**Figure 3E; Supplementary File 10**). Two metabolites, hippurate (**Figure 3F**) and Trimethylamine
325 N-oxide (TMAO) (**Figure 3G**), were identified as products of gut microbial metabolism and both were
326 lower in patients with cirrhosis compared to HC, and lower in ACLF than in SC or DC (**Figure 3F-G**;
327 **Supplementary Figure 2**). Contrasting urinary metabolites with the percentage proportion of
328 bacterial genus showed that *Enterococcus* abundance was negatively correlated with several

329 metabolites including hippurate and TMAO, while *Ruminococcus*, *Coprococcus*, and *Roseburia* were
330 positively correlated with hippurate and TMAO (**Figure 3H; Supplementary Figure 3**).

331 Similar differences were seen in plasma metabolites with significant differences between cirrhosis
332 cohorts and HC (**Supplementary Figure 4A; Supplementary File 11**) amongst several plasma
333 metabolites (**Supplementary Figure 4B-G**). Similarly, *Enterococcus* abundance correlated with
334 changes in a number of plasma metabolites (**Supplementary Figure 4H**).

335 These findings show a pattern characterised by elevated concentrations of primary bile acids in
336 plasma and reduced quantities of recognised microbial metabolites in the urine among cirrhosis
337 patients with more advanced disease.

338

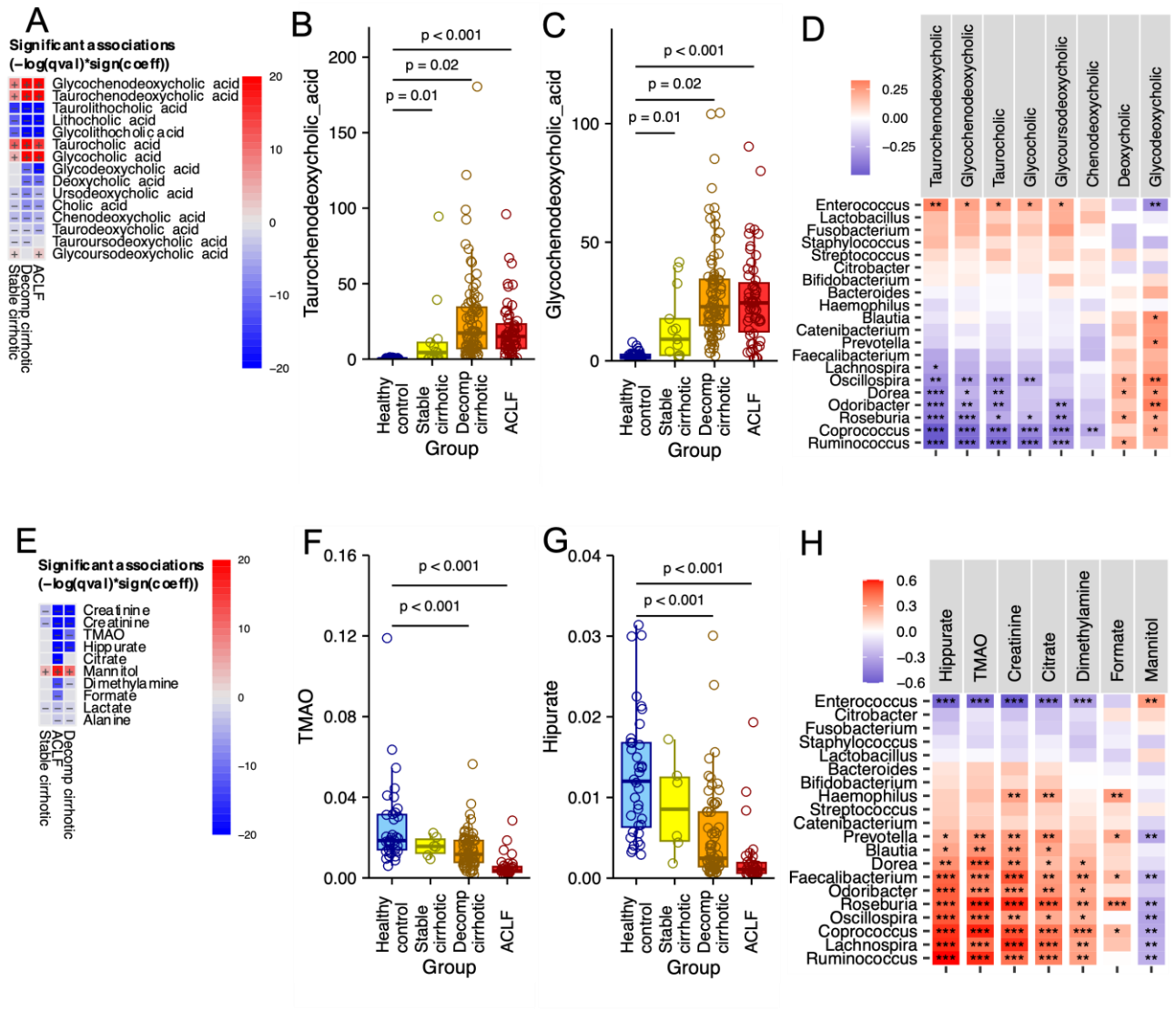

Figure 3: Plasma bile acids, urinary metabolites, and correlations with abundance of faecal bacterial genera.

(A) The heatmap displays MaAslin2 analysis results of significant associations between plasma bile acid concentrations and cirrhosis cohorts using HC as a reference. The two plasma bile acids with the strongest positive effect size for cirrhosis severity determined by MaAslin2 using HC as a reference and shown as box and dot plots were (B) Taurochenodeoxycholic acid and (C) Glycochenodeoxycholic acid. (D) Pearson correlations between the normalised relative abundance of the top twenty most abundant faecal bacterial genera (comprising 98% of the microbiota) and normalised plasma bile acid concentrations showing bile acids with significant correlations. (E) The heatmap displays MaAslin2

349 analysis results of significant associations between urinary metabolite concentrations and cirrhosis
350 severity using HC as a reference. The two urinary metabolites with the strongest negative effect size
351 for cirrhosis severity determined by MaAslin2 using HC as a reference and shown as box and dot plots
352 were (F) Trimethylamine N-oxide (TMAO) and (G) Hippurate. (H) Pearson correlations between the
353 normalised relative abundance of the top twenty most abundant faecal bacterial genera (comprising
354 98% of the microbiota) and normalised urinary metabolite concentrations showing metabolites with
355 significant ($P < 0.05$) correlations. Full correlations shown in Supplementary Figure 3 and 4.

356 **2.5. Clinical variables link to overall microbiota profiles, with further associations in advanced**
357 **cirrhosis of *Enterococcus* with antibiotic usage and resistance profiles**

358 Next, we carried out an exploratory analysis to determine how clinical parameters might be
359 associated with gut microbiota composition, using the envfit function, focusing on each clinical
360 variable and overall microbiota beta-diversity. The ten clinical variables with the strongest
361 association with faecal microbiota composition were plotted overlaying an NMDS plot
362 (**Supplementary Figure 1).** Several clinical factors correlated with microbiota composition, with
363 conventional measures of cirrhosis severity showing the strongest association (**Supplementary**
364 **Figure 1, Supplementary File 7**). Composite clinical scores are used to classify cirrhosis severity and
365 for prognostication. Of those included in this analysis, ACLF grade, MELD score, Child-Pugh grade and
366 score, and UKELD score were all associated with microbiota composition, in keeping with the study
367 phenotyping of the cirrhosis cohorts, i.e. SC, DC, and ACLF.

368 Antibiotic use, oral food intake, and lactulose use were clinical variables identified as both having an
369 association with microbiota composition, and considered likely to have a direct influence on the gut
370 microbiota **(Supplementary File 2)**. Differential abundance testing was carried out using MaAslin2
371 for antibiotic use, oral food intake, and lactulose use along with cirrhosis severity was included within
372 the MaAslin2 model to adjust for covariance (**Supplementary File 12**). Antibiotic use, oral food intake,
373 lactulose use, all showed significant effects on differential abundance of genus within the patient
374 cohort when adjusted for covariance. Comparing the genus with the large difference in abundance
375 in cirrhosis patients receiving or not receiving enteral intake, *Roseburia* abundance was lower in
376 patients not receiving nutrition *via* enteral routes (normal oral intake and by enteral tube feeding),

377 while *Enterococcus* abundance was higher (**Figure 4A**). Similarly, *Roseburia* abundance was lower in
378 patients receiving antibiotics, while *Enterococcus* abundance was higher (**Figure 4B**). Results were
379 unchanged when excluding the 5 patients only receiving rifaximin as antibiotic treatment. Lactulose
380 use was associated with a higher relative abundance of *Bifidobacterium* within the patient cohort
381 between those receiving lactulose and those not (Figure 4E). *Enterococcus* remained significantly
382 higher abundance in DC and ACLF severity groups compared to HC when adjusted for antibiotic use,
383 oral food intake indicating an independent effect of all three factors on *Enterococcus* abundance
384 (**Supplementary Table 2**).

385 The cirrhosis group as a whole received a total of 19 different types of antibiotics (**Figure 4F;**
386 **Supplementary Table 2.** The most frequently used antibiotics were piperacillin/tazobactam (Tazocin)
387 (33 patients) and 16 Meropenem (16 patients) totalling 37% of patients while 48 (36%) received no
388 antibiotics. The remaining 17 antibiotics were given to 6 or fewer patients with 8 antibiotics only
389 given to one patient. To visualise the complexities of this antibiotic administration, data was
390 visualised as a heatmap with patients clustered by antibiotic use and antibiotics clustered by co-
391 occurrence (**Figure 4C**). Associations of gut bacterial genus differential abundance with all individual
392 antibiotic administration was tested in a MaAslin2 model with only piperacillin/tazobactam (Tazocin)
393 and meropenem individually associated with abundance of *Enterococcus* (**Supplementary Table 8**
394 **Figure 4C**). Five out of 48 patients not currently receiving antibiotics also showed higher *Enterococcus*
395 relative abundance (**Figure 4C**). This cirrhosis cohort included a range of aetiologies, however, cause
396 of cirrhosis did not significantly associate with gut microbiota composition. Rather, cirrhosis severity,
397 antibiotics, and nutritional intake use was the primary factor that co-associated with a dominant
398 *Enterococcus* gut microbiota signature in patients with most severe disease i.e. DC and ACLF
399 (**Supplementary figure 7A,B**).

400 To probe *Enterococcus* traits in more detail, five isolates obtained from five different patient faecal
401 samples (one sample from the DC cohort and four from the ACLF cohort) underwent whole genome
402 sequencing and were identified as *Enterococcus faecium*. Comparing the similarities of these 5 novel
403 isolates with an additional publicly available 185 *E. faecium* genomes (retrieved from the NCBI
404 GenBank database) using midpoint rooted maximum-likelihood tree showed a diversity of *E. faecium*
405 genomes with no single clonal group colonising patients with cirrhosis indicating that the *E. faecium*

406 isolates did not originate from the same source (**Figure 4D**). The five *E. faecium* cirrhosis isolate
407 genomes were aligned against virulence-related gene profiles, antibiotic resistance genes, and bile
408 resistance genes (**Figure 4E**). These isolates contained between 12 and 17 of the 20 antibiotic
409 resistance genes analysed (**Figure 4E**); 5 genes encoding aminoglycoside resistance, 7 *van* genes
410 encoding vancomycin resistance, 3 encoding macrolides resistance, 2 encoding tetracycline
411 resistance, and 2 trimethoprim resistance. The two bile acid resistance genes *bsh* and *gltK* were
412 present in all patient isolates, and in the genomes of 95% of all 190 isolates from public databases
413 (**Figure 4F**).

414 Taken together, these data indicate that clinical factors such as reduced enteral nutritional intake
415 and exposure to the broad-spectrum beta-lactam antibiotics piperacillin/tazobactam (Tazocin) and
416 meropenem were strongly linked to higher levels of *Enterococcus* and decreased abundance of
417 commensal genera in patients with cirrhosis. Broad-spectrum beta-lactam antibiotics are commonly
418 administered to DC and ACLF patients as part of their treatment regimen. *Enterococcus* isolates
419 obtained and sequenced from these patients were identified as *E. faecium* and were found to encode
420 various antibiotic and bile acid resistance genes, indicating potential bacterial survival mechanisms
421 and pathogenicity.

422

423

424

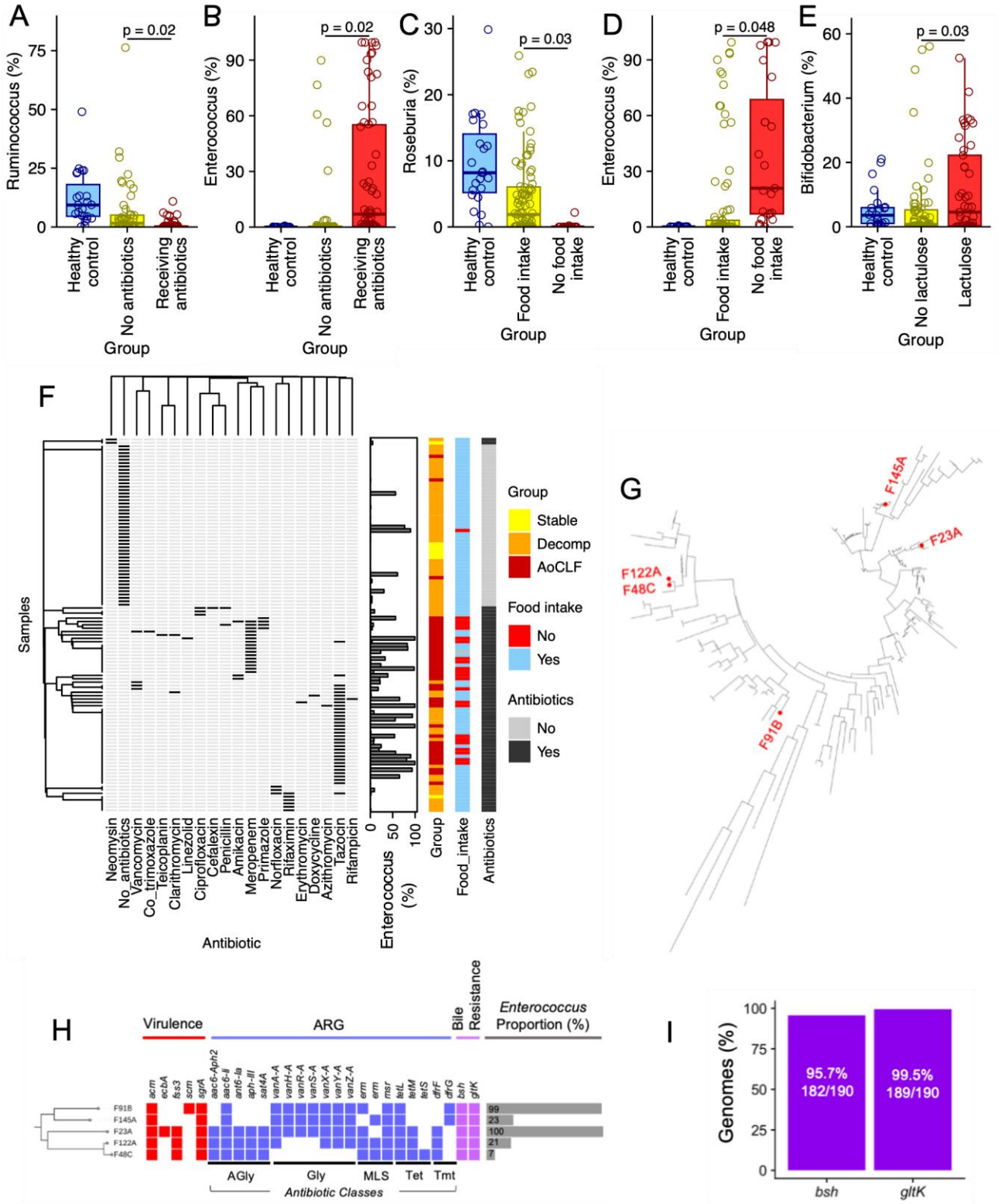

Figure 4: Oral food intake, receiving antibiotics, and *Enterococcus faecium* genomic data.

427 The differentially abundant genera with the strongest negative and positive effect sizes for antibiotics
428 with patients not receiving antibiotics as the reference were (A) *Ruminococcus* and (B) *Enterococcus*.
429 The differentially abundant genera with the strongest negative and positive effect sizes for nutritional
430 intake with patients not receiving enteral as the reference were (C) *Roseburia* and (D) *Enterococcus*.
431 The differentially abundant genera with the strongest positive effect size for lactulose use with
432 patients not receiving lactulose as the reference was (E) *Bifidobacterium*. (F) Clustered individual
433 antibiotics received by patients with cirrhosis cohort, nutritional status, and relative abundance of
434 *Enterococcus* in each sample. (G) A midpoint rooted maximum-likelihood tree consisted of 190
435 *Enterococcus faecium* genomes, including 5 novel *E. faecium* isolates obtained from cirrhosis
436 patients, as highlighted in the tree. (H) Novel *E. faecium* genomes (n=5) from cirrhosis patients
437 aligned with virulence-related gene profiles, virulence (using VFDB), ARG (Antibiotic Resistance
438 Genes; using ARG-ANNOT) and bile resistance genes (*bsh* and *gltK*), accordingly. Proportion of
439 *Enterococcus* (genus level; based on 16S rRNA sequence data) in the corresponding faecal samples
440 was also indicated in the horizontal bar chart. (I) Proportion of detectable bile resistance genes (%)
441 *bsh* and *gltK* in 190 *E. faecium* genomes, suggesting that these two genes belong to the core genome
442 of *E. faecium*.

443 **2.6. Faecal microbiota and markers of bacterial translocation, intestinal and systemic**
444 **inflammation, and monocyte exhaustion.**

445 To explore links between gut barrier dysfunction and translocation of intestinal bacteria and/or their
446 products from the gut into the systemic circulation, we determined the number of copies of 16S rDNA
447 in whole blood from cirrhosis patients and HC. The number of copies of 16S rDNA in the blood was
448 lowest in HC in keeping with a degree of 'physiological translocation' and displayed a stepwise
449 increase with severity of cirrhosis (**Figure 5A**). To identify associations with the faecal microbiota, we
450 correlated copies of 16S rDNA in the blood against percentages of bacterial genera (**Figure 5B**), with
451 *Enterococcus* most strongly positively correlated (**Figure 5C**), and *Lachnospira* most negatively
452 correlated (**Figure 5C**). Faecal calprotectin as a conventional marker of non-specific gut mucosal
453 inflammation also showed a stepwise increase with cirrhosis severity compared to HC (**Figure 5D**).
454 Faecal calprotectin was positively correlated with relative abundance of *Enterococcus* **(Figure 5E**) and
455 negatively correlated with *Lachnospira* (**Figure 5E**).

456 The innate immune function of CD14+ monocytes isolated from peripheral blood obtained from
457 cirrhosis patients and HCs was assessed by stimulation with TLR 2/4/9 agonists *in vitro*, with
458 unstimulated controls, and the percentage of Tumour necrosis factor-alpha (TNF- α), Interleukin-6
459 (IL-6), and monocyte human leukocyte antigen-DR (HLA-DR) positive monocytes identified by flow
460 cytometry. Monocytes from DC and ACLF patients showed attenuated proinflammatory responses
461 (TNF-α and IL-6) to Pam3, LPS and CpG challenge, indicating reduced innate responses to pathogen-
462 induced TLR signalling pathways. (**Supplementary Figure 1**). To identify cirrhosis-associated
463 alterations in monocyte function and associations with factors linked to the microbiota, the
464 percentage of TNF-a or IL-6 positive monocytes were correlated with copies of 16S rDNA in whole
465 blood, faecal calprotectin, and the twenty faecal genera with the highest overall abundance (**Figure**
466 **5I; Supplementary Figure 6**). The number of copies of bacterial DNA in whole blood positively
467 correlated with the percentage of IL-6 positive unstimulated monocytes, while the number of genera
468 positively correlated with the percentage of TNF-alpha and IL-6 positive LPS-stimulated monocytes
469 (**Figure 5I**). *Lachnospira* showed positive associations and *Enterococcus* negative associations with
470 the percentage of TNF-alpha and IL-6 positive LPS stimulated monocytes (**Figure 5J**) and *Enterococcus*
471 with TNF-alpha positive Pam3 stimulated monocytes (**Figure 5IK**).

472 These findings reveal contrasting associations between *Enterococcus* and other commensal bacterial
473 genera, such as *Lachnospira*, on markers of intestinal permeability, intestinal and systemic
474 inflammation, and monocyte innate immune function.

475

476

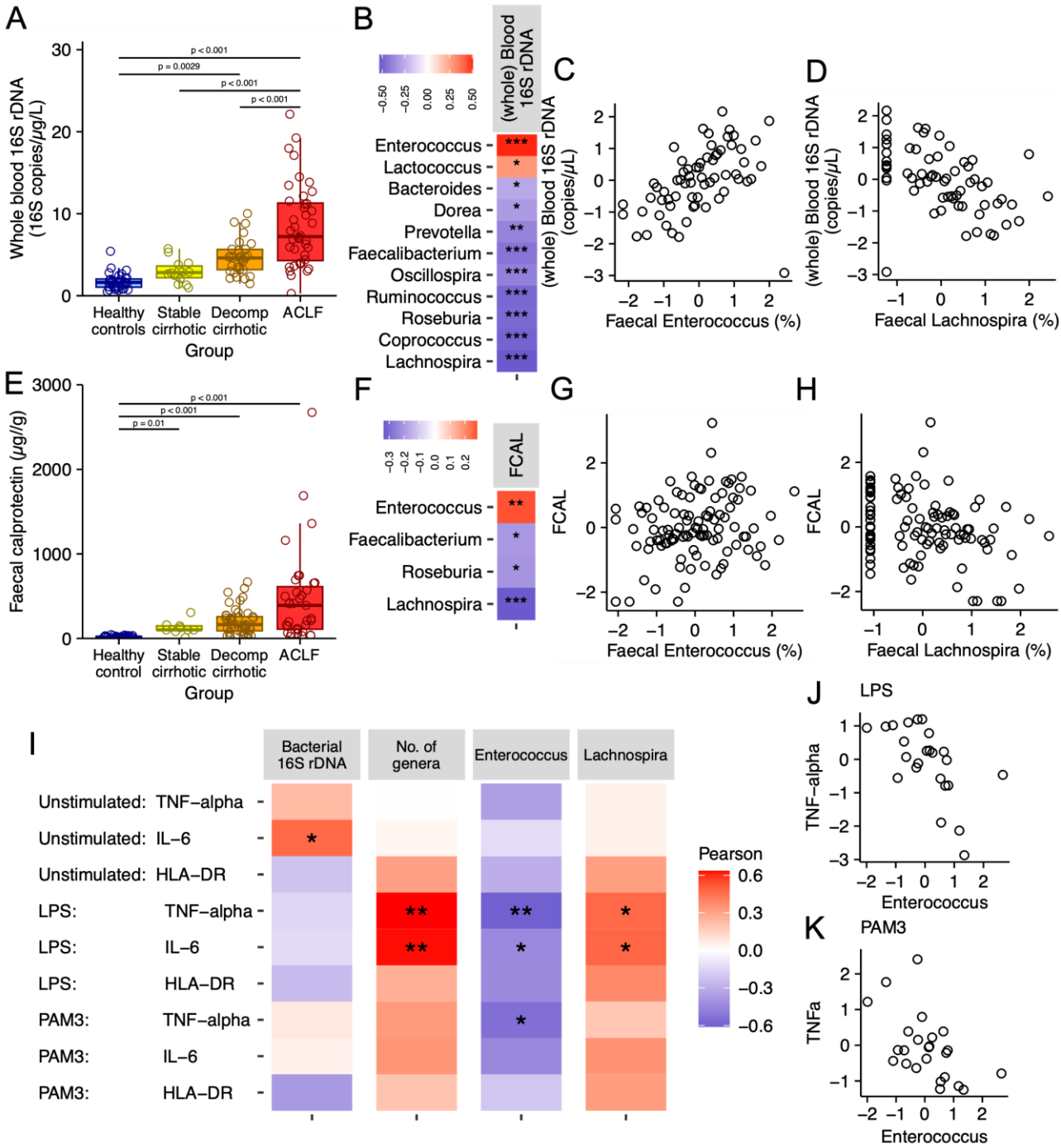

Figure 5. Markers of intestinal permeability and intestinal inflammation and correlations of stimulated monocyte activation with (whole) blood 16S rDNA and faecal microbiota.

(A) Copies of 16S rDNA in participant blood by cirrhosis severity vs HC. (B) Significant correlations between copies of 16S rDNA in participant blood and percentage of genera in the faecal microbiota. (C) Scatter plot of copies of 16S rDNA in blood against faecal *Enterococcus* for each participant. (D)

483 Scatter plot of copies of 16S rDNA in blood against faecal *Lachnospira* for each participant. (E) Faecal
484 calprotectin concentration by cirrhosis severity vs HC. (F) Significant correlations between faecal
485 calprotectin concentration and percentage of genera in the faecal microbiota. (G) Scatter plot of
486 faecal calprotectin concentration against faecal *Enterococcus* percentage for each participant. (H)
487 Scatter plot of faecal calprotectin concentration against faecal *Lachnospira* percentage for each
488 participant. (I) Percentage of monocytes showing TNF-α and IL-6 production and HLA-DR expression
489 in response to antigen stimuli (LPS/TLR-4; Pam3CSK4/TLR-2, CpG/TLR-9) correlated separately with
490 whole blood 16S rDNA, number of faecal genera, faecal *Enterococcus* percentage and faecal
491 *Lachnospira* percentage. Stars (*) indicate statistical significance ($P < 0.05$) after adjustment for
492 multiple testing. (J) Scatter plot of percentage of TNF-alpha positive LPS stimulated monocytes
493 against faecal *Enterococcus* percentage for each participant. (K) Scatter plot of percentage of TNF-
494 alpha positive PAM3 stimulated monocytes against faecal *Enterococcus* percentage for each
495 participant.

496

497

498 # 3. Discussion

499 We found higher relative abundance of *Enterococcus* in the gut microbiota of patients with cirrhosis,
500 particularly in those with advanced disease and receiving broad spectrum antibiotics, accompanied
501 by a lower abundance of obligate anaerobic commensal genera. This shift is consistent with patterns
502 seen in other conditions with compromised intestinal barrier function, such as preterm infants
503 (Hufnagel et al., 2007) and Graft-versus-Host Disease (Garrett, 2020), as well as other studies in ACLF
504 (Lee et al., 2024a, 2024b; Solé et al., 2021). These findings suggest that *Enterococcus*, an
505 opportunistic pathogen, may exploit disrupted gut microbial communities and diminished
506 colonisation resistance to thrive, especially in advanced disease states with multiple gut microbiota
507 modulating treatments.

508 Multiple factors may contribute to the selection and proliferation of resident *Enterococcus* strains in
509 the gut of cirrhosis patients. Antibiotic use is one such factor, as many of the patients with high
510 *Enterococcus* levels had received broad-spectrum beta-lactam antibiotics like
511 Piperacillin/tazobactam or meropenem. These antibiotics are commonly administered to
512 hospitalised DC and ACLF patients for treating suspected infections, often before culture results are
513 available, and *Enterococcus* exhibits intrinsic resistance to beta-lactam antibiotics (Zapun et al.,
514 2008), potentially providing a selective advantage. Additionally, the *E. faecium* isolates in this study
515 encoded genes conferring bile acid resistance (Zhang et al., 2013), which may further facilitate
516 persistence in the bile-rich environment characteristic of advanced cirrhosis (Kakiyama et al., 2013).
517 Elevated intestinal luminal bile acids in cirrhosis, particularly primary bile acids, can alter the gut
518 microbial environment (Ridlon et al., 2013), often reducing bile-sensitive commensals like *Roseburia*
519 and providing an ideal niche for *Enterococcus* to overgrow.

520 This relative overgrowth of *Enterococcus* in the gut microbiota, especially strains with virulence genes
521 like *acm* and *sgrA* (encoded in all strains isolated from this study cohort), which enhance adhesion
522 and translocation, presents significant clinical implications. These strains may be associated with
523 systemic infections that can exacerbate cirrhosis-related complications, such as progression from a
524 stable state to DC and ACLF (Hendrickx et al., 2009; Nallapareddy et al., 2008). Moreover, bacterial
525 sepsis is a significant complication in patients with cirrhosis, an increasing recognition of the threat

526 of antimicrobial resistance (Piano et al., 2019; Wong et al., 2021). Carriage of multidrug resistant
527 strains (as indicated by our genomic analysis) may contribute to greater clinical complication
528 episodes by way of hepatic decompensation, organ failure and mortality rates, due to increased
529 translocation of *Enterococcus* via a dysfunctional and inflamed gut barrier into the bloodstream.
530 Furthermore, as *Enterococcus* appears to dominate more severely ill patients to the exclusion of
531 other potential pathogens, this pattern raises questions about its source. Genomic analysis showed
532 divergent strains of *E. faecium* were present in patients rather than any common clonal lineages,
533 which would be the case if multiple patients had acquired the *E. faecium* from each other or from
534 the same hospital environment. This indicated that the *E. faecium* are more likely to represent
535 resident gut strains already in the patient rather than nosocomial infections. Further investigation
536 involving a larger number of isolates will be valuable to confirm these findings.

537 As faecal *Enterococcus* abundance increased, we observed a corresponding significant decline in key
538 commensal bacterial genera including *Roseburia*, *Ruminococcus*, *Coprococcus*, and *Faecalibacterium*,
539 with many ACLF patients showing an almost complete relative absence. These genera are essential
540 for SCFA production, such as butyrate (Flint et al., 2012), which supports intestinal barrier integrity.
541 The loss of these beneficial microbes is a common feature in cirrhosis (Acharya and Bajaj, 2019) that
542 is linked to the development of gut barrier failure, pathological microbial translocation and cirrhosis-
543 associated immune dysfunction. Their decline appears to be further exacerbated by common
544 therapeutic factors in the treatment of advanced cirrhosis, such as the use of broad-spectrum
545 antibiotics, which impact antibiotic-sensitive species (Zimmermann and Curtis, 2019), and a reliance
546 on fibre-deficient diets, particularly among patients dependent on enteral or parenteral nutrition
547 (present in 45% of the ACLF group). These diets lack the necessary fermentable dietary fibre to
548 sustain SCFA-producing microbes, worsening microbial disruption and potentially contributing to gut
549 permeability.

550 This microbiota disruption is mirrored by lower urinary levels of metabolites like hippurate which is
551 a products of beneficial microbial metabolism and fibre-rich diets (Lees et al., 2013) and TMAO, which
552 is a microbial byproduct or metabolising nutrients including choline, betaine, and carnitine found in
553 meat, eggs, and fish (Pallister et al., 2017). Hippurate production, often associated with microbial
554 metabolism of phenolic compounds in fruits and vegetables, was positively correlated with

555 *Ruminococcus*, further linking microbial loss with decreased metabolic activity. Similarly, TMAO -
556 produced via hepatic conversion of trimethylamine (TMA), itself a microbial metabolite from dietary
557 sources like carnitine and lecithin - was also reduced, indicating either a reduction in dietary
558 substrates or a loss of the bacteria producing TMA or potentially a loss of liver function to convert
559 TMA into TMAO (van den Berg et al., 2023). Reduced *Ruminococcus* abundance correlated with
560 decreased urinary TMAO, reflecting not only microbial shifts but also dietary limitations and potential
561 hepatic enzymatic changes (FMO1 and FMO3) seen in advanced cirrhosis (Organ et al., 2020)
562 (Gatarek and Kaluzna-Czaplinska, 2021; Williams et al., 2010). These data suggest that microbial and
563 dietary disturbances may jointly contribute to the metabolic and immune challenges observed in
564 cirrhosis progression.

565 Further, we noted that patients with cirrhosis exhibited elevated plasma bile acids, especially
566 glycochenodeoxycholic and TCDCA, which correlated with cirrhosis severity. This increase likely
567 stems from impaired hepatic bile acid uptake and reduced conversion to secondary bile acids due to
568 the loss of deconjugating genera like *Lachnospiraceae* and *Ruminococcaceae* genera that were
569 significantly depleted in this cirrhosis cohort (Vital et al., 2019). This impaired conversion could
570 further favour the persistence of *Enterococcus*, as elevated primary bile acids can disrupt the gut
571 microbial ecosystem and inhibit commensal bacteria.

572 Consistent with microbial translocation in cirrhosis, we observed elevated copies of 16S rDNA in the
573 systemic circulation of patients, correlating with cirrhosis severity and reflecting gut barrier
574 dysfunction (Albillos et al., 2022). This microbial translocation, along with elevated faecal calprotectin
575 concentrations, and associated breakdown of gut barrier function and integrity in cirrhosis (Riva et
576 al., 2020), linking with loss of key butyrate-producing microbes like *Ruminococcus* and
577 *Faecalibacterium* genera in DC and ACLF patients (Fagan et al., 2015) (Bach Knudsen et al., 2018).
578 Reduced faecal short-chain fatty acids have been previously reported (Jin et al., 2019; Wang et al.,
579 2023), and a reduced capacity to ferment dietary fibre in cirrhosis patients compared to healthy
580 controls (Jin et al., 2019). *Enterococcus*, which correlated strongly with 16S rDNA copies in the blood,
581 and gut inflammation markers like faecal calprotectin, indicates its likely role in gut inflammation and
582 immune activation in these patients. In cirrhosis, the progressive loss of intestinal barrier integrity
583 allows MAMPs, and viable bacteria, like *Enterococcus*, to translocate into the bloodstream, triggering

584 systemic inflammation and further impairing immune function (Tilg et al., 2022). Indeed, previous
585 work in mice indicates that *E. faecium* triggers colonic cytokine expression, which appears to be strain
586 dependent (Seishima et al., 2019) and related to elevated faecal cytokine levels and other markers
587 of gut barrier dysfunction in DC patients (Riva et al., 2020). Conversely, *Lachnospira* were markedly
588 reduced in cirrhosis patients (Abdugheni et al., 2022), potentially resulting in the loss of the
589 protective role of SCFAs that dampen mucosal immune activation such as through activation and
590 maturation of T regulatory cells (Y et al., 2013). Coupled with impaired immune responses to
591 pathogen-associated TLR signalling, as observed in the CD14+ monocytes of cirrhotic patients, this
592 suggests a vicious cycle of gut perturbations, immune dysfunction, and bacterial translocation that
593 exacerbates systemic inflammation.

594 Interestingly, despite the widespread antibiotic use in the DC and ACLF patients, *Bifidobacterium*
595 persisted in the microbiota of patients with cirrhosis. This genus is typically considered sensitive to
596 antibiotic use (Moubareck et al., 2005), so its resilience here may be due to the frequent use of
597 lactulose, a non-absorbable disaccharide laxative often prescribed to prevent or treat hepatic
598 encephalopathy. Lactulose acts as a prebiotic, providing a substrate that *Bifidobacterium* can
599 metabolise, thereby promoting its growth. Recent studies have shown lactulose can elevate
600 *Bifidobacterium* levels in cirrhosis patients, which inhibited the antibiotic-resistant pathobiont
601 vancomycin-resistant *E. faecium* through potential mechanisms including lowering the luminal pH
602 and via acetate production (Odenwald et al., 2023). Our results add to these recent findings that
603 lactulose supplementation could help support *Bifidobacterium* populations in patients with cirrhosis
604 (Odenwald et al., 2023).

605 From a therapeutic perspective, restoring the gut microbiota toward a healthier balance, or
606 "eubiosis", could mitigate the cycle of immune dysfunction and prevent cirrhosis-related
607 complications (Tranah et al., 2021). Dietary or microbial interventions, such as prebiotics, probiotics,
608 or microbiome-targeted treatments, could offer a promising approach. While faecal microbiota
609 transplantation is currently being trialled (e.g. ClinicalTrials.gov: NCT02862249, NCT06461208,
610 NCT04932577), it carries risks for patients with advanced cirrhosis, where highly personalised or
611 targeted microbiome interventions may be safer (Cibulková et al., 2021) and use of Cefepime to
612 protect anaerobes in gut vs Pip Taz / meropenem. Probiotics or prebiotics aimed at restoring

613 beneficial taxa lost in cirrhosis, such as *Roseburia*, could help inhibit *Enterococcus* overgrowth,
614 reinforce intestinal barrier integrity, and reduce inflammation. However, these approaches are not
615 available yet clinically or commercially, and significant investment and development is needed to
616 bring such novel, next-generation microbiome-modulating therapies to benefit this patient
617 population. This highlights the urgency for better antimicrobial stewardship and the development of
618 rapid diagnostics that can better target potential pathogens while reducing the use of broad
619 spectrum antibiotics and deescalating to avoid prolonged courses of exposure.

620 Our findings raise the possibility that the overgrowth of *Enterococcus* and loss of commensal
621 microbiota may not merely correlate with disease severity, and associated conventional therapies
622 such as the use of antibiotics and absence of a dietary fibre may also contribute to disease
623 progression. However, our cross-sectional study design and single time-point sampling limit our
624 ability to infer causality. Longitudinal studies, combined with animal models, could further clarify
625 whether *Enterococcus* contributes to pathological processes in cirrhosis or is an opportunistic
626 response to the disrupted gut environment. Additionally, refined antibiotic strategies, possibly
627 reducing the selective pressure for *Enterococcus*, alongside targeted dietary support to foster
628 beneficial microbes, may represent viable options to improve outcomes for these high-risk patients.

629

630

4. Methods

Study participants & biological sampling

Patient participants were stratified and phenotyped according to clinically relevant groups based on the severity and time course of their underlying cirrhosis, degree of hepatic decompensation, and presence and extent of hepatic and extra-hepatic organ failure at the time of sampling. These groups were stable cirrhosis (SC; n=15), decompensated cirrhosis (DC; n=55) and acute-on-chronic liver failure (ACLF; n=57), with a separately recruited healthy control cohort (HC; n=40). SC was defined as having Child Pugh A grade(score) of A(5-6). DC was defined by the acute development of 1 or more major complications of cirrhosis, including ascites, HE, variceal haemorrhage, and bacterial infection. ACLF was defined and graded according to the number of organ failures in concordance with criteria reported in the CANONIC study (Arroyo et al., 2015; Moreau et al., 2013). Main exclusion criteria included pregnancy, hepatic or non-hepatic malignancy (HCC within Milan criteria were included), pre-existing immunosuppressive states, replicating HBV/HCV/HIV infection, and known inflammatory bowel disease. Further details are provided in the Supplementary section.

Patients were consecutively recruited at King's College Hospital after admission to the ward or when reviewed in the hepatology out-patient clinic, through an observational study and a clinical trial. The observational study was granted approval by the NHS Health Research Authority NRES Committee London Westminster [REC reference: 12/LO/1417] and local sponsor Research and Development department (KCH12-126). Ethical approval for the interventional trial was obtained from NHS Health Research Authority NRES Committee South Central-Oxford C (Bristol) [REC reference: 14/SC/0088] and from the Medicines and Healthcare products Regulatory Agency for Clinical Trial Authorisation [EudraCT number: 2013-004708-20; ClinicalTrials.gov NCT02019784]. The studies were conducted in compliance with the principles of the Declaration of Helsinki (1996), principles of Good Clinical Practice, Research Governance Framework and where relevant, the Medicines for Human Use (Clinical Trial) Regulations. Clinical service users and caregivers were fully consulted and involved in the design of both the study and the trial, and were given opportunities to review and feedback on overall set-up, delivery and practical aspects, including input into development of all participant facing documents. Only baseline pre-intervention data from the clinical trial participants are used in

659 this manuscript. Fully informed consent was obtained from all participants. Some participants eligible
660 for this study were unable to provide informed consent due to cognitive impairment arising from HE
661 and permission from a legal representative was sought.

662 Patient participants, or their legal representative in the case of incapacitation of a potential
663 participant, provided written informed consent within 48 hours of presentation. Patients were
664 managed according to standard evidence-based protocols and guidelines (European Association for
665 the Study of the Liver., 2018). Patient and Public Involvement and Engagement was undertaken with
666 a patient advisory group to determine acceptability of the studies, provided their perspective on
667 study design, informational material, measures to minimise participation burden and agreeing on a
668 dissemination plan of the findings.

669 Patient participants were stratified into and phenotyped according to clinically relevant groups based
670 on the severity and time course of their underlying cirrhosis, degree of stability and hepatic
671 decompensation, and presence and extent of hepatic and extra-hepatic organ failure at the time of
672 sampling. These groups were stable cirrhosis, acutely decompensated cirrhosis (AD) and acute-on-
673 chronic liver failure (ACLF), with a separately recruited healthy participant control cohort. AD was
674 defined by the acute development of 1 or more major complications of cirrhosis, including ascites,
675 hepatic encephalopathy, variceal haemorrhage, and bacterial infection. ACLF was defined and graded
676 according to the number of organ failures in concordance with criteria reported in the CANONIC study
677 (Arroyo et al., 2016; Moreau et al., 2013).

678 Demographic, clinical, and biochemical metadata were collected at the time of biological sampling.
679 Standard clinical composite scores used for risk stratification and prognostication included the Child-
680 Pugh score (Pugh et al., 1973), model for end-stage liver disease (MELD) (Kim et al., 2008), United
681 Kingdom model for end-stage liver disease (UKELD) (Asrani and Kim, 2010), and Chronic Liver Failure
682 Consortium-acute decompensation (CLIF-C AD) (Jalan et al., 2015). Healthy controls aged >18 years
683 (n = 40) were recruited to establish reference values for the various assays performed. Exclusion
684 criteria for healthy controls were body mass index <18 or >27; pregnancy or active breastfeeding, a
685 personal history of thrombotic or liver disease; chronic medical conditions requiring regular primary
686 or secondary care review and/or prescribed pharmacotherapies; or current use of anticoagulants,

687 platelet function inhibitors, or oral contraceptives, and no exposure to antibiotics in the previous 6
688 months.

689 **Faecal, urine and blood sample collection and preparation**

690 Plasma samples for bile acid and cytokine profiling were obtained within 24 hours of admission to
691 hospital. Blood was drawn into ethylenediaminetetraacetic acid (EDTA) containing vacuum tubes (BD
692 Vacutainer, Franklin Lakes, NJ, USA). Plasma fractions were collected from these tubes following
693 incubation at room temperature and centrifugation at 2,000 x g for 10 minutes at 4°C. Plasma aliquots
694 were stored immediately at -80°C until further analysis. Whole blood from EDTA tubes was aliquoted
695 into sterile microtubes for and stored immediately at -80°C for bacterial DNA quantification.

696 Faecal samples for 16S rRNA sequencing and calprotectin quantification were obtained within 48
697 hours of admission to hospital using non-treated sterile universal tubes. Faecal samples were kept at
698 4˚C without any preservative and within 6 hours were aliquoted into 1 gram vials for storage at -80˚C.

699 Serum and urine samples were prepared for NMR analyses using standardised protocols (Dona et al.,
700 2014).

701 **Isolation and quality assessment of faecal bacterial DNA**

702 Bacterial DNA was isolated from all faecal samples obtained. This was performed utilising an ISOLATE
703 II Faecal DNA Kit (Bioline, London, UK; BIO-52082). Faecal samples were thawed from -80ºC at room
704 temperature for up to 30 minutes. 150mg of faecal material (crude faecal from each faecal sample)
705 was added directly to a Bashing Beads Lysis Tube (Zymo Research, Orange County, California, USA)
706 and rapidly lysed by bead beating in a vortex, without the use of organic denaturants or proteinases.
707 The DNA was then bound, isolated and purified using spin columns. To optimise the DNA binding
708 step, β-mercaptoethanol (Sigma-Aldrich, Saint Louis, Missouri, USA) was added to eliminate
709 deoxyribonucleases released during cell lysis, by reducing the disulfide bonds within the
710 deoxyribonuclease enzymes. This prevents enzymatic digestion of the DNA during its extraction
711 procedure, increasing the overall yield. The eluted DNA, free of contaminants and enzyme inhibitors,
712 is then used for downstream molecular biology applications including genotyping and sequencing.
713 Extracted DNA concentration and purity were measured using a NanoDrop spectrophotometer

714 (Thermo Fisher Scientific, Australia). Samples with DNA concentrations below the dynamic range of
715 the NanoDrop spectrophotometer were analysed using Qubit High-Sensitivity (HS) dsDNA Assay kit
716 (Life Technologies, Australia).

717 **Faecal 16S rRNA gene amplicon library preparation and sequencing**

718 Amplicons were generated using the method as described previously (Jervis-Bardy et al. 2015). Full
719 details of the library preparation and sequencing protocol are provided in Appendix section 9.3. In
720 brief, barcoded amplicon libraries for the bacterial community analysis on the Illumina MiSeq
721 platform were generated using degenerate primers targeting the V1 and V3 hypervariable regions of
722 the bacterial 16S rRNA gene and Nextera XT index kit (Illumina, Inc., Victoria, Australia).

723 Amplicons were generated using fusion degenerate primers 27 F (5'-
724 TCGTCGGCAGCGTCAGATGTGTATAAGAGACAGAGRGTTTGATCMTGGCTCAG-3') and 519R (5'-
725 GTCTCGTGGGCTCGGAGATGTGTATAAGAGACAGGTNTTACNGCGGCKGCTG-3') with ligated overhang
726 Illumina adapter consensus sequences in italic text. In brief, the initial PCR reactions were performed
727 on a Veriti 96-well Thermal Cycler (Life Technologies, Australia). The PCR reactions were performed
728 in the following programme: initiation enzyme activation at 95°C for 3 min, followed by 25 cycles
729 consisting of denaturation at 95°C for 30 sec, annealing at 55°C for 30 sec and extension at 72°C for
730 30 sec. After 25 cycles, the reaction was completed with a final extension of 7 min at 72°C.

731 The Illumina Nextera XT Index kit (Illumina Inc., San Diego. CA, USA) with dual 8-base indices were
732 used to allow for multiplexing. Two unique indices located on either end of the amplicon were chosen
733 based on the Nextera dual-indexing strategy. To incorporate the indices to the 16S amplicons, PCR
734 reactions were performed on a Veriti 96-well Thermal Cycler (Life Technologies, Australia). Cycling
735 conditions consisted of one cycle of 95°C for 3 min, followed by eight cycles of 95°C for 30 sec, 55°C
736 for 30 sec and 72°C for 30 sec, followed by a final extension cycle of 72°C for 5 min.

737 Prior to library pooling, the barcoded libraries were quantified using the Qubit dsDNA HS Assay Kit
738 (Life Technologies, Carlsbad, CA, USA). Results from this quantification step (amplicon concentration)
739 were used in downstream processing to eliminate contamination. The libraries were sequenced by 2
740 × 300 bp paired-end sequencing on the MiSeq platform using MiSeq v3 Reagent Kit (Illumina) at the

741 Flinders Genomics Facility, Adelaide, Australia. All sequence data generated have been submitted to
742 the Sequence Read Archive (Archive 2014).

743 **16S rRNA amplicon sequencing analysis**

744 The 16S rRNA amplicon sequencing raw reads are deposited in NCBI SRA under project
745 PRJNA1223169. Sequencing reads were analysed using OTU clustering approach via QIIME v1.9.1 as
746 previously described (Kiu et al., 2019). Briefly, raw paired-end reads were firstly merged using PEAR
747 v0.9.6 with -q 30 option (Zhang et al., 2014). Next, quality filtering is performed with
748 split_libraries_fastq.py (QIIME) with -q 29 to retain high-quality reads (Caporaso et al., 2010).
749 Subsequently, chimera removal was performed via chimera identification
750 (identify_chimeric_seqs.py) and chimera sequence removal script (filter_fasta.py). OTU clustering
751 was run via open reference approach (pick_open_reference_otus.py) which does not discard
752 unassigned reads, based on SILVA_132 16S rRNA database optimised for use with QIIME (Quast et
753 al., 2013). BIOM outputs of taxonomic profiles generated from QIIME were then exported using
754 MEGAN v6 (Huson et al., 2016).

755 The sequencing output of 135 samples included one sample containing only 405 sequences and this
756 was discarded from further analysis. The remaining 134 samples contained a mean of 13,905
757 sequences per sample (Standard Deviation 6,497) with a minimum of 2,761 and maximum of 38,637
758 sequences per sample. Rarefaction curves were generated using the rarecurve function in the vegan
759 package (Oksanen, 2017) in R to confirm acceptable levels of sequencing depth. Raw data was
760 normalised using the Deseq2 (Love et al., 2014) package in R using the
761 varianceStabilizingTransformation function.

762 ***Enterococcus* isolation, genomic DNA extraction, Whole Genome Sequencing (WGS) and analysis**

763 Selected faecal samples (~20mg) were subject to serial dilutions in sterile PBS before spread-plating
764 on Slanetz and Bartley agar (Thermo Scientific) for selection of Enterococcus colonies (Slanetz and
765 Bartley, 1957). Subsequently, distinct deep-red coloured colonies, presumably Enterococci, on the
766 agar plates were picked and re-streaked once on fresh Slanetz and Bartley agar after incubation at
767 40°C for 24h. Re-streaked agar plates were then incubated at 40°C for a further 24h to ensure isolate

768 purity prior to overnight culturing in 10ml Brain Heart Infusion media at 40°C to generate sizable
769 bacterial pellets for subsequent genomic DNA extraction. Genomic DNA extraction on the
770 Enterococcus isolates was performed using FastDNA Spin Kit for Soil (MP Biomedicals) as per
771 manufacturer's instructions as described previously (Gooch et al., 2021).

772 Sequencing library was prepared via a modified Illumina Nextera Flex low input tagmentation
773 approach as described previously (Baker et al., 2021; Gooch et al., 2021). Genomic DNA samples were
774 sequenced on Illumina NextSeq 500 with read lengths of 150bp (paired-end).

775 Sequencing reads were quality-filtered and adapter-removed using fastp v0.20.0 with -q 20 option
776 (Chen et al., 2018). Next, short reads were assembled using Unicycler v0.4.9 via primary de novo
777 assembler SPAdes v3.11.1 prior to read polishing via Pilon v1.22. Contigs of length <500 bp were then
778 removed from all draft genome assemblies (Bankevich et al., 2012; Walker et al., 2014; Wick et al.,
779 2017). Taxonomic assignment (Enterococcus faecium) to novel draft genome assemblies were
780 performed using GTDB-Tk v1.5.1 (Chaumeil et al., 2020).

781 A total of 185 E. faecium complete genome assemblies were retrieved from NCBI Genome database
782 (December 2021) for comparison purposes. Together with 5 novel *E. faecium* genomes (n=200), a
783 core gene alignment was generated using Panaroo v1.2.8 with --merge_paralogs option while SNP
784 variants were next extracted by snp-sites v2.3.3 (Page et al., 2016; Tonkin-Hill et al., 2020).
785 Subsequently, a phylogenetic tree was reconstructed via FastTree v2.1 -gtr (-nt) model based on the
786 alignment of core genome SNPs and visualised on iTOL v6 (Letunic and Bork, 2019; Price et al., 2009).

787 Gene search was performed via ABRicate v1.0.1 with --mincov=90 and--minid=90, using databases
788 ARG-ANNOT v6 (AMR genes) and VFDB (Virulence genes) (Gupta et al., 2014; Liu et al., 2019).
789 Nucleotide sequences of bile-salt resistance genes bsh (Accession: AY260046.1) and gltK (Accession:
790 EFF34375.1) were retrieved from GenBank (Benson et al., 2018).

791 **Faecal calprotectin quantification**

792 Faecal calprotectin was measured from frozen faecal samples using a commercially available enzyme-
793 linked immunosorbent assay (Bühlmann Laboratories AG, Schönenbuch, Switzerland) that measures
794 calprotectin in a quantitative manner. This was undertaken in a conventional hospital clinical

795 laboratory (ISO 15189 accredited) with regular interval review of standard operating procedures and
796 equipment calibration. Extraction buffer was added to aliquots of 50mg raw faeces at a
797 weight/volume ratio of 1:50 and homogenised by vortexing for 30 minutes. 2mL of the homogenate
798 was then centrifuged in a microcentrifuge for 5 min at 3000 g. Following centrifugation, the
799 calprotectin ELISA was performed using an automated Grifols Triturus® platform. The ELISA plate is
800 coated with a monoclonal capture antibody highly specific to the calprotectin heterodimeric and
801 polymeric complexes. After incubation, washing, a second incubation with a specific detection
802 antibody, and a further washing step, tetramethylbenzidine (blue colour formation) followed by a
803 stop solution (change to yellow colour) are added by the Triturus. The absorption was determined at
804 an optical density of 450 nm. The linear range of the test was 10-600 µg calprotectin/g faeces with
805 concentration-dependent intra- and inter-assay coefficients of between 2-5% and 4-8%, respectively.

806 **Whole blood 16S ribosomal DNA quantification**

807 The method for quantifying whole blood 16S ribosomal DNA has been previously published in detail
808 (Vergis et al., 2017). Prior to 16S rRNA gene PCR analysis, frozen whole blood samples were thawed
809 to room temperature over a 15-minute period. Mutanolysin (Sigma, St. Louis, Missouri, USA) was
810 added directly to the whole-blood sample; 10µL of 10U/µL enzyme was added for every 200µL of
811 blood being processed, and the sample was incubated for 30 minutes at 37°C.

812 DNA isolation was performed using a total whole blood volume of 200µL per sample. 19µL of
813 10mg/ml lysozyme and 1µL glycogen (Thermo Fisher Scientific; R0561), the latter to aid precipitation,
814 was added to the sample and placed in a water bath at 37°C for 30 minutes. A modified protocol from
815 the QIAmp DNA Blood Mini Kit (Qiagen, Inc., Valencia, CA) was then followed: 200µL of AL buffer was
816 added and the sample vortexed. 20µL of Proteinase K (Thermo Fisher Scientific; EO0491) was then
817 added and then incubated at 56°C for 1 hour in a heat block. After incubation, 200µL of 100% ethanol
818 was added and the resulting lysates were loaded onto the QIAamp DNA Mini kit spin columns.

819 The columns were then centrifuged at 6,000 x g for one minute, and 500µL wash buffer AW1 added,
820 again centrifuged at 6,000 x g for one minute. 500µL wash buffer AW2 was then added, centrifuged
821 at 13,000 x g for three minutes. 50µL of pre-warmed AE elution buffer was added with 5 minutes
822 waiting time, then centrifuged at 13,000 x g for one minute to obtain the DNA extracts. To maximise

823 extraction, the eluate was reapplied to the spin column and centrifuged at 6,000 x g for one minute.
824 PBS and healthy control whole blood PCR were included to quality check for contamination from the
825 process.

826 Real-time polymerase chain reaction (PCR) was used to assess the quantity of bacterial DNA by
827 comparing to known standards. The primers and TaqMan probes were the well-characterized RW01
828 and DG74 primers and TaqMan RDR245 universal probe (synthesized at Applied Biosystems, Foster
829 City, CA) and have been described previously (Jordan and Durso, 2005) with a 380bp 16S rRNA gene
830 target. This target is located in the highly conserved region of 16S bacterial rRNA gene in order to
831 detect the majority of bacterial species found in clinical samples.

832 The forward primer sequence was: 5'-AAC TGG AGG AAG GTG GGG AT3' and the reverse primer
833 sequence was 5'-AGG AGG TGA TCC AAC CGC A-3'. The TaqMan probe sequence was 5'-(6-FAM)-TA
834 CAA GGC CCG GGA ACG TAT TCA CCG-(TAMRA)-3'. Each well contained 5.5µL sterile water (UV
835 irradiated), 1µL RW01 forward primer (10uM), 1µL DG74 reverse primer (10µM), 0.5ul RDR245
836 TaqMan probe (10µM), 10µL of TaqMan Gene Expression Master Mix (Invitrogen; 4369016) and 2µL
837 of sample containing the DNA eluate.

838 A 96 well plate was used and each sample was run in triplicate, and for each plate that was run blank
839 wells were included, a negative control (sterile PBS) and various healthy control samples spiked with
840 a known quantity of E.coli and then serially diluted to generate a standard curve to allow absolute
841 quantification to be calculated. Accordingly, for each PCR run, a standard curve was generated by
842 including a healthy control blood sample which was spiked with known quantities of E.coli (0.4ng,
843 0.04ng, 0.004ng, 0.0004ng, 0.00004ng) using serial 10-fold dilutions and a negative control, also all
844 run in triplicate, and were put through the same DNA extraction process. Any sample displaying a
845 positive signal at or below the level of the negative control was considered negative. Any triplicate
846 group with readings >1 copy cycle apart was considered unreliable and discarded; otherwise, the
847 mean reading was calculated.

848 A StepOnePlus PCR instrument (Invitrogen) was used for real-time PCR, with an initial 2 minutes at
849 50°C and 10-minute denaturation at 95°C, followed by 40 cycles of 15 seconds at 95°C, 30 seconds at
850 60C (annealing) and 1 minute at 72°C (extension). Fluorescence measurements on the PCR

851 instrument were collected during the extension phase of each cycle, and a cycle threshold (C_T) value
852 for each sample and control (including a blank well) was calculated by determining the point at which
853 the fluorescence exceeded the threshold limit, which was set automatically. These values were
854 compared with the *E. coli* standards to obtain a relative quantification of bacterial DNA detected in
855 the whole blood and control samples. Standard curves were generated, and concentrations
856 interpolated in Prism, version 7.0 (GraphPad, La Jolla, CA, USA) The results were extrapolated to
857 picograms of bacterial DNA per millilitre of whole blood.

858 **Plasma cytokine analyses**

859 Plasma cytokines were measured as follows: IL-2, IL-4, IL-6, IL-8, IL-10, IL-12 p70, IL-13, IFN-ɣ, IL1β
860 and TNF-α using an electro-chemiluminescence platform (Meso Scale Discovery (MSD)). Samples
861 were run in duplicate on U-PLEX Proinflam Combo 1 Human™ plates (Cat# K15049K-1, MSD,
862 Gaithersburg, MD). This was conducted according to the manufacturer's protocol. The plate was
863 immediately read on a SECTOR(r) Imager (MSD, Gaithersburg, MD).

864 **Plasma bile acid profiling**

865 Bile acid (BA) profiling was done using an in-house high performance liquid chromatography tandem
866 mass spectrometry (LC-MS/MS) assay modified from published methodology (Tagliacozzi et al.,
867 2003). The method uses an Acentis fusedcore C18 analytical column (15064.6 mm, particle size 2.7
868 mm, Sigma-Aldrich) on a Jasco LC2000 series HPLC system attached to an API 3200 triple quadrupole
869 mass spectrometer (Applied Biosystems, Cheshire, UK). Mobile phases comprised (A) methanol or
870 (B) deionised H2O, each containing 5 mM ammonium acetate (w/v) and 0.012% formic acid (v/v).
871 Negative ion mass spectra of the fractionated BAs were recorded in multiple reaction-monitoring
872 mode. Data were captured using Analyst Software version 1.4.2 (Applied Biosystems) and
873 quantitation carried out by peak area analysis corrected to internal standards (a2,2,4,4,d4-
874 deoxycholic acid for each of the bile acid chemistries; unconjugated, glycine- and taurine-
875 conjugated). The method was linear between 0.1 and 10 mmol/L for all BAs and their conjugates with
876 coefficients of variation (CV %) of 1.5–6.8% at the lower limit of quantitation (0.1 mmol/L). The inter-
877 assay CV was 3.6–8.0%.

878 **Plasma ^{1}H NMR spectroscopy**

879 All plasma samples were prepared according to the previously published papers by Dona et al. and
880 Trovato et al. (Dona et al., 2014; Trovato et al., 2021)[TOO ADD]. ^{1}H NMR spectra were acquired on
881 a Bruker 600 MHz (Avance III) spectrometer, operating at a ^{1}H frequency of 600.16 MHz (14.1 Tesla)
882 at 310K using a 5 mm BBI probe and an automated Sample Jet system (Bruker Biospin, Rheinstetten,
883 Germany). Full explanation of processing is given in the Supplementary section.

884 **Urine ^{1}H NMR spectroscopy**

885 Urinary NMR data were acquired at the Centre for Biomolecular Spectroscopy, King's College London,
886 using a Bruker 600-MHz (AVANCE NEO) NMR spectrometer with a 1H/13C/15N TCI Prodigy (nitrogen-
887 cooled) probe (Bruker, Billerica, USA) as previously described (Bajaj et al., 2019). Pulse-collect NMR
888 data sets were acquired using PURGE water suppression (Le Guennec et al., 2017) and J-resolved
889 NMR sequences. Signal intensities of metabolite regions were obtained using intellibucketing within
890 Wiley KnowItAll® Informatics, Metabolomics Edition v17.0, Wiley Science Solutions, Colorado, USA.
891 NMR spectral regions excluded from the analysis at the outset were 10.0 ppm and 4.5-5.0 ppm
892 (residual water region). Selected intellibucket regions were manually adjusted to incorporate specific
893 metabolite peaks. The binned NMR spectral data outputted from Wiley KnowItAll® Informatics
894 Metabolomics Edition v17.0 were also analysed using MetaboAnalyst v4.0 program (Chong et al.,
895 2018) and exported to the Quadram Institute. Details can be found in the Supplementary section.

896 **Monocyte intracellular cytokine staining**

897 Monocyte intracellular cytokine staining was undertaken using thawed PBMCs from patients with
898 liver disease and at a density of 0.5 millions cells per ml. Cells were either stimulated with TLR2
899 (Pam3CSK4 5ug/ml), Invivogen, France), TLR4 (LPS 100 ng/ml), or TLR9 (CpG 10ug/ml) (Invivogen,
900 France) for 4 hours, or left unstimulated. Monocytes were identified using monoclonal antibodies for
901 surface markers: CD14 PE-Cy7, CD16 APC-H7 (BD Biosciences, UK) and HLA-DR PerCP (ThermoFisher
902 Scientific, UK). Intracellular cytokines were measured using protein transport inhibitor containing
903 monensin, permeabilization/fixation buffer and monoclonal antibodies TNF-α APC and IL-6 PE (BD
904 Biosciences, UK). Percentage positivity in CD14+ monocytes compared with isotype controls (APC

905 mouse IgG1; PE rat IgG2a) were assessed by flow cytometry as previously described (Antoniades et
906 al., 2014). The gating strategy that was employed is shown in Supplementary Figure 1.

907 **Statistical and bioinformatic analyses**

908 For microbiota diversity analysis the number of genera in each sample and the Inverse Simpson
909 diversity was calculated using the specnumber and the diversity functions on genus level taxonomic
910 sequence data in the vegan package (version 2.6-4) in R using raw sequence count data (Oksanen,
911 2017). Differences in alpha-diversity between cirrhosis severity and HC groups was tested with an
912 ANOVA using the aov function in R. Post-hoc pairwise comparisons were determined using the
913 TukeyHSD function in R.

914 To visualise clustering of gut bacterial communities between participants non-metric
915 multidimensional scaling (NMDS) based on a Bray-Curtis distance matrix and using the metaMDS
916 function with k = 3 dimensions contained within the vegan package (version 2.6-4) (Oksanen, 2017).
917 The influence of cirrhosis severity group compared to HC on participant microbiota clustering was
918 tested using a PERMANOVA test using the adonis2 function in the vegan package (version 2.6-4) with
919 a total of 10,000 permutations. Pairwise comparison of clustering of the three cirrhosis severity and
920 HC groups was compared using the pairwiseAdonis function in the pairwiseAdonis package (Martinez
921 Arbizu, 2020).

922 To explore the effect size and significance of associations between clinical metadata variables and
923 beta-diversity of the microbiota within patient samples the envfit function in the vegan package was
924 used to test associations of clinical metadata variables on NMDS ordination calculated using Bray-
925 Curtis dissimilarity after 10,000 permutations. In total, 76 clinical metadata variables were included
926 in the envfit analysis to explore their associations with the gut microbiota composition with three
927 samples excluded during analysis due to missing data (Supplementary File 2). The P-values for
928 combined continuous and factor variables were corrected for multiple comparisons using an FDR
929 adjustment (Benjamini–Hochberg procedure). For visualisation the R2 for the forty significant
930 variables were presented as a bar plot while an arbitrary top ten clinical variables explaining the
931 highest amount of variance (R2) were plotted as an overlay on a NMDS plot of the individual gut
932 microbiota data using the ggplot2 package.

933 Associations between the relative abundance of individual bacterial genera and individual clinical
934 metadata variables were tested using the MaAsLin2 package (Mallick et al., 2021). For genus
935 abundance analysis MaAsLin2 was run with default parameters including multiple testing correction
936 using Benjamini-Hochberg FDR with a significance threshold on adjusted P-values of 0.25 as
937 recommended by the developers. Exceptions to default parameters included an applied minimum
938 prevalence of 0.01 and abundance cut-off of 0.01. Each metadata variable was tested individually.
939 For genus differential abundance analysis cirrhosis severity was included at a Fixed Effect with the
940 HC group as the reference group. For genus differential abundance analysis using antibiotic use, oral
941 food intake, and lactulose use each variable was tested individually. Positive associations were
942 identified antibiotic use, oral food intake, and lactulose and these three variables where combined
943 and tested together as Fixed Effects in a multivariable analysis for the final analysis.

944 Differential analysis of bile acid concentrations was performed using MaAsLin2 with multiple testing
945 correction using Benjamini-Hochberg FDR with a significance threshold on adjusted P-values of 0.25
946 as recommended by the developers. Exceptions to default parameters included no minimum
947 concentration nor abundance cut-off, CLR as the normalisation method and no transformation used.
948 Differential analysis of urinary metabolite and plasma concentrations were analysed using MaAsLin2
949 run with default parameters including multiple testing correction using Benjamini-Hochberg FDR with
950 a significance threshold on adjusted P-values of 0.25 as recommended by the developers. Exceptions
951 to default parameters included no minimum concentration nor abundance cut-off, and no
952 normalisation nor transformation used. The BestNormalize package (version 1.9.1.9000) (Peterson,
953 2021; Peterson and Cavanaugh, 2020) in R was used to optimally normalise each metabolite
954 individually before analysis using the bestnorm function. The method used to transform each variable
955 included in (Supplementary Table 3).

956 For correlation analysis the variables were normalised using the bestnorm function from the
957 bestNormalize package (version 1.9.1.9000). The method used to transform each variable included
958 in (Supplementary Table 4). Pearson correlations were used with statistical significance corrected for
959 multiple testing across genus tested using the False Discovery Rate method.

960

961 # 5. Acknowledgements

962 We are grateful to all the patient participants and healthy volunteers for agreeing to take part in this
963 study, and to the clinical and liver research teams at King's College Hospital for facilitating
964 recruitment, collecting metadata and biological sample collection. We thank the King's College
965 Hospital Charity and a generous donation from a Liver Service User, and the Foundation for Liver
966 Research for funding. Sequencing analysis was supported in part by the NBI Research Computing
967 through the provision of a High Performance Computing. The authors thank the Centre for
968 Biomolecular Spectroscopy funded by the Wellcome Trust and British Heart Foundation (ref.
969 202767/Z/16/Z and IG/16/2/32273).

970

971

972

6. References

Abdugheni, R., Wang, W.-Z., Wang, Y.-J., Du, M.-X., Liu, F.-L., Zhou, N., Jiang, C.-Y., Wang, C.-Y., Wu, L., Ma, J., Liu, C., Liu, S.-J., 2022. Metabolite profiling of human-originated Lachnospiraceae at the strain level. iMeta 1, e58. https://doi.org/10.1002/imt2.58

Acharya, C., Bajaj, J.S., 2019. Altered Microbiome in Patients With Cirrhosis and Complications. Clin Gastroenterol Hepatol 17, 307–321. https://doi.org/10.1016/j.cgh.2018.08.008

Adak, A., Khan, M.R., 2019. An insight into gut microbiota and its functionalities. Cell Mol Life Sci 76, 473–493. https://doi.org/10.1007/s00018-018-2943-4

Albillos, A., de Gottardi, A., Rescigno, M., 2020. The gut-liver axis in liver disease: Pathophysiological basis for therapy. J Hepatol 72, 558–577. https://doi.org/10.1016/j.jhep.2019.10.003

Albillos, A., Martin-Mateos, R., Van der Merwe, S., Wiest, R., Jalan, R., Álvarez-Mon, M., 2022. Cirrhosis-associated immune dysfunction. Nat Rev Gastroenterol Hepatol 19, 112–134. https://doi.org/10.1038/s41575-021-00520-7

Alexopoulou, A., Agiasotelli, D., Vasilieva, L.E., Dourakis, S.P., 2017. Bacterial translocation markers in liver cirrhosis. Ann Gastroenterol 30, 486–497. https://doi.org/10.20524/aog.2017.0178

Antoniades, C.G., Khamri, W., Abeles, R.D., Taams, L.S., Triantafyllou, E., Possamai, L.A., Bernsmeier, C., Mitry, R.R., O'Brien, A., Gilroy, D., Goldin, R., Heneghan, M., Heaton, N., Jassem, W., Bernal, W., Vergani, D., Ma, Y., Quaglia, A., Wendon, J., Thursz, M., 2014. Secretory leukocyte protease inhibitor: a pivotal mediator of anti-inflammatory responses in acetaminophen-induced acute liver failure. Hepatology 59, 1564–1576. https://doi.org/10.1002/hep.26933

Arroyo, V., Moreau, R., Jalan, R., Ginès, P., EASL-CLIF Consortium CANONIC Study, 2015. Acute-on-chronic liver failure: A new syndrome that will re-classify cirrhosis. J Hepatol 62, S131-143. https://doi.org/10.1016/j.jhep.2014.11.045

Arroyo, V., Moreau, R., Kamath, P.S., Jalan, R., Ginès, P., Nevens, F., Fernández, J., To, U., García-Tsao, G., Schnabl, B., 2016. Acute-on-chronic liver failure in cirrhosis. Nat Rev Dis Primers 2, 16041. https://doi.org/10.1038/nrdp.2016.41

Asrani, S.K., Kim, W.R., 2010. Organ allocation for chronic liver disease: model for end-stage liver disease and beyond. Curr Opin Gastroenterol 26, 209–213. https://doi.org/10.1097/MOG.0b013e32833867d8

Bach Knudsen, K.E., Lærke, H.N., Hedemann, M.S., Nielsen, T.S., Ingerslev, A.K., Gundelund Nielsen, D.S., Theil, P.K., Purup, S., Hald, S., Schioldan, A.G., Marco, M.L., Gregersen, S., Hermansen, K., 2018. Impact of Diet-Modulated Butyrate Production on Intestinal Barrier Function and Inflammation. Nutrients 10, 1499. https://doi.org/10.3390/nu10101499

Bajaj, J.S., Heuman, D.M., Hylemon, P.B., Sanyal, A.J., White, M.B., Monteith, P., Noble, N.A., Unser, A.B., Daita, K., Fisher, A.R., Sikaroodi, M., Gillevet, P.M., 2014. Altered profile of human gut microbiome is associated with cirrhosis and its complications. Journal of Hepatology 60, 940–947. https://doi.org/10.1016/j.jhep.2013.12.019

Bajaj, J.S., Reddy, K.R., Tandon, P., Garcia-Tsao, G., Kamath, P.S., O'Leary, J.G., Wong, F., Lai, J., Vargas, H., Thuluvath, P.J., Subramanian, R.M., Pena-Rodriguez, M., Sikaroodi, M., Thacker, L.R., Gillevet, P.M., 2022. Association of serum metabolites and gut microbiota at hospital admission with nosocomial infection development in patients with cirrhosis. Liver Transpl 28, 1831–1840. https://doi.org/10.1002/lt.26552

1015 Bajaj, J.S., Ridlon, J.M., Hylemon, P.B., Thacker, L.R., Heuman, D.M., Smith, S., Sikaroodi, M., Gillevet,
1016 P.M., 2012. Linkage of gut microbiome with cognition in hepatic encephalopathy. Am J Physiol
1017 Gastrointest Liver Physiol 302, G168-175. https://doi.org/10.1152/ajpgi.00190.2011
1018 Bajaj, J.S., Salzman, N., Acharya, C., Takei, H., Kakiyama, G., Fagan, A., White, M.B., Gavis, E.A., Holtz,
1019 M.L., Hayward, M., Nittono, H., Hylemon, P.B., Cox, I.J., Williams, R., Taylor-Robinson, S.D.,
1020 Sterling, R.K., Matherly, S.C., Fuchs, M., Lee, H., Puri, P., Stravitz, R.T., Sanyal, A.J., Ajayi, L., Le
1021 Guennec, A., Atkinson, R.A., Siddiqui, M.S., Luketic, V., Pandak, W.M., Sikaroodi, M., Gillevet,
1022 P.M., 2019. Microbial functional change is linked with clinical outcomes after capsular fecal
1023 transplant in cirrhosis. JCI Insight 4, e133410, 133410.
1024 https://doi.org/10.1172/jci.insight.133410
1025 Baker, D.J., Aydin, A., Le-Viet, T., Kay, G.L., Rudder, S., de Oliveira Martins, L., Tedim, A.P., Kolyva, A.,
1026 Diaz, M., Alikhan, N.-F., Meadows, L., Bell, A., Gutierrez, A.V., Trotter, A.J., Thomson, N.M.,
1027 Gilroy, R., Griffith, L., Adriaenssens, E.M., Stanley, R., Charles, I.G., Elumogo, N., Wain, J.,
1028 Prakash, R., Meader, E., Mather, A.E., Webber, M.A., Dervisevic, S., Page, A.J., O'Grady, J.,
1029 2021. CoronaHiT: high-throughput sequencing of SARS-CoV-2 genomes. Genome Medicine
1030 13, 21. https://doi.org/10.1186/s13073-021-00839-5
1031 Bankevich, A., Nurk, S., Antipov, D., Gurevich, A.A., Dvorkin, M., Kulikov, A.S., Lesin, V.M., Nikolenko,
1032 S.I., Pham, S., Prjibelski, A.D., Pyshkin, A.V., Sirotkin, A.V., Vyahhi, N., Tesler, G., Alekseyev,
1033 M.A., Pevzner, P.A., 2012. SPAdes: a new genome assembly algorithm and its applications to
1034 single-cell sequencing. J Comput Biol 19, 455–477. https://doi.org/10.1089/cmb.2012.0021
1035 Benson, D.A., Cavanaugh, M., Clark, K., Karsch-Mizrachi, I., Ostell, J., Pruitt, K.D., Sayers, E.W., 2018.
1036 GenBank. Nucleic Acids Research 46, D41–D47. https://doi.org/10.1093/nar/gkx1094
1037 Caballero-Flores, G., Pickard, J.M., Núñez, G., 2023. Microbiota-mediated colonization resistance:
1038 mechanisms and regulation. Nat Rev Microbiol 21, 347–360. https://doi.org/10.1038/s41579-
1039 022-00833-7
1040 Caporaso, J.G., Kuczynski, J., Stombaugh, J., Bittinger, K., Bushman, F.D., Costello, E.K., Fierer, N.,
1041 Peña, A.G., Goodrich, J.K., Gordon, J.I., Huttley, G.A., Kelley, S.T., Knights, D., Koenig, J.E., Ley,
1042 R.E., Lozupone, C.A., McDonald, D., Muegge, B.D., Pirrung, M., Reeder, J., Sevinsky, J.R.,
1043 Turnbaugh, P.J., Walters, W.A., Widmann, J., Yatsunenko, T., Zaneveld, J., Knight, R., 2010.
1044 QIIME allows analysis of high-throughput community sequencing data. Nat Methods 7, 335–
1045 336. https://doi.org/10.1038/nmeth.f.303
1046 Chaumeil, P.-A., Mussig, A.J., Hugenholtz, P., Parks, D.H., 2020. GTDB-Tk: a toolkit to classify genomes
1047 with the Genome Taxonomy Database. Bioinformatics 36, 1925–1927.
1048 https://doi.org/10.1093/bioinformatics/btz848
1049 Chen, S., Zhou, Y., Chen, Y., Gu, J., 2018. fastp: an ultra-fast all-in-one FASTQ preprocessor.
1050 Bioinformatics 34, i884–i890. https://doi.org/10.1093/bioinformatics/bty560
1051 Chong, J., Soufan, O., Li, C., Caraus, I., Li, S., Bourque, G., Wishart, D.S., Xia, J., 2018. MetaboAnalyst
1052 4.0: towards more transparent and integrative metabolomics analysis. Nucleic acids research
1053 46. https://doi.org/10.1093/nar/gky310
1054 Cibulková, I., Řehořová, V., Hajer, J., Duška, F., 2021. Fecal Microbial Transplantation in Critically Ill
1055 Patients—Structured Review and Perspectives. Biomolecules 11, 1459.
1056 https://doi.org/10.3390/biom11101459
1057 Da Silva, H.E., Teterina, A., Comelli, E.M., Taibi, A., Arendt, B.M., Fischer, S.E., Lou, W., Allard, J.P.,
1058 2018. Nonalcoholic fatty liver disease is associated with dysbiosis independent of body mass
1059 index and insulin resistance. Sci Rep 8, 1466. https://doi.org/10.1038/s41598-018-19753-9

1060 D'Amico, G., Bernardi, M., Angeli, P., 2022. Towards a new definition of decompensated cirrhosis.
1061 Journal of Hepatology 76, 202–207. https://doi.org/10.1016/j.jhep.2021.06.018
1062 Dona, A.C., Jiménez, B., Schäfer, H., Humpfer, E., Spraul, M., Lewis, M.R., Pearce, J.T.M., Holmes, E.,
1063 Lindon, J.C., Nicholson, J.K., 2014. Precision high-throughput proton NMR spectroscopy of
1064 human urine, serum, and plasma for large-scale metabolic phenotyping. Anal Chem 86, 9887–
1065 9894. https://doi.org/10.1021/ac5025039
1066 Dubinkina, V.B., Tyakht, A.V., Odintsova, V.Y., Yarygin, K.S., Kovarsky, B.A., Pavlenko, A.V., Ischenko,
1067 D.S., Popenko, A.S., Alexeev, D.G., Taraskina, A.Y., Nasyrova, R.F., Krupitsky, E.M., Shalikiani,
1068 N.V., Bakulin, I.G., Shcherbakov, P.L., Skorodumova, L.O., Larin, A.K., Kostryukova, E.S.,
1069 Abdulkhakov, R.A., Abdulkhakov, S.R., Malanin, S.Y., Ismagilova, R.K., Grigoryeva, T.V., Ilina,
1070 E.N., Govorun, V.M., 2017. Links of gut microbiota composition with alcohol dependence
1071 syndrome and alcoholic liver disease. Microbiome 5, 141. https://doi.org/10.1186/s40168-
1072 017-0359-2
1073 European Association for the Study of the Liver., 2018. EASL Clinical Practice Guidelines for the
1074 management of patients with decompensated cirrhosis. J Hepatol 69, 406–460.
1075 https://doi.org/10.1016/j.jhep.2018.03.024
1076 Fagan, K.J., Rogers, G.B., Melino, M., Arthur, D.M., Costello, M.-E., Morrison, M., Powell, E.E., Irvine,
1077 K.M., 2015. Ascites Bacterial Burden and Immune Cell Profile Are Associated with Poor Clinical
1078 Outcomes in the Absence of Overt Infection. PLoS One 10, e0120642.
1079 https://doi.org/10.1371/journal.pone.0120642
1080 Flint, H.J., Scott, K.P., Duncan, S.H., Louis, P., Forano, E., 2012. Microbial degradation of complex
1081 carbohydrates in the gut. Gut Microbes 3, 289–306. https://doi.org/10.4161/gmic.19897
1082 Garrett, W.S., 2020. Enterococcus in Graft-versus-Host Disease. N Engl J Med 382, 1064–1066.
1083 https://doi.org/10.1056/NEJMcibr1915978
1084 Gatarek, P., Kaluzna-Czaplinska, J., 2021. Trimethylamine N-oxide (TMAO) in human health. EXCLI J
1085 20, 301–319. https://doi.org/10.17179/excli2020-3239
1086 Ghosh, S., Whitley, C.S., Haribabu, B., Jala, V.R., 2021. Regulation of Intestinal Barrier Function by
1087 Microbial Metabolites. Cellular and Molecular Gastroenterology and Hepatology 11, 1463–
1088 1482. https://doi.org/10.1016/j.jcmgh.2021.02.007
1089 Gooch, H.C.C., Kiu, R., Rudder, S., Baker, D.J., Hall, L.J., Maxwell, A., 2021. Enterococcus innesii sp.
1090 nov., isolated from the wax moth Galleria mellonella. Int J Syst Evol Microbiol 71, 005168.
1091 https://doi.org/10.1099/ijsem.0.005168
1092 Gupta, S.K., Padmanabhan, B.R., Diene, S.M., Lopez-Rojas, R., Kempf, M., Landraud, L., Rolain, J.-M.,
1093 2014. ARG-ANNOT, a New Bioinformatic Tool To Discover Antibiotic Resistance Genes in
1094 Bacterial Genomes. Antimicrob Agents Chemother 58, 212–220.
1095 https://doi.org/10.1128/AAC.01310-13
1096 Hendrickx, A.P.A., van Luit-Asbroek, M., Schapendonk, C.M.E., van Wamel, W.J.B., Braat, J.C.,
1097 Wijnands, L.M., Bonten, M.J.M., Willems, R.J.L., 2009. SgrA, a nidogen-binding LPXTG surface
1098 adhesin implicated in biofilm formation, and EcbA, a collagen binding MSCRAMM, are two
1099 novel adhesins of hospital-acquired Enterococcus faecium. Infect Immun 77, 5097–5106.
1100 https://doi.org/10.1128/IAI.00275-09
1101 Hernaez, R., Solà, E., Moreau, R., Ginès, P., 2017. Acute-on-chronic liver failure: an update. Gut 66,
1102 541–553. https://doi.org/10.1136/gutjnl-2016-312670
1103 Horvatits, T., Drolz, A., Roedl, K., Rutter, K., Ferlitsch, A., Fauler, G., Trauner, M., Fuhrmann, V., 2017.
1104 Serum bile acids as marker for acute decompensation and acute-on-chronic liver failure in

1105 patients with non-cholestatic cirrhosis. Liver Int 37, 224–231.
1106 https://doi.org/10.1111/liv.13201
1107 Hsu, C.L., Schnabl, B., 2023. The gut–liver axis and gut microbiota in health and liver disease. Nat Rev
1108 Microbiol 21, 719–733. https://doi.org/10.1038/s41579-023-00904-3
1109 Huang, D.Q., Terrault, N.A., Tacke, F., Gluud, L.L., Arrese, M., Bugianesi, E., Loomba, R., 2023. Global
1110 epidemiology of cirrhosis — aetiology, trends and predictions. Nat Rev Gastroenterol Hepatol
1111 20, 388–398. https://doi.org/10.1038/s41575-023-00759-2
1112 Hufnagel, M., Liese, C., Loescher, C., Kunze, M., Proempeler, H., Berner, R., Krueger, M., 2007.
1113 Enterococcal colonization of infants in a neonatal intensive care unit: associated predictors,
1114 risk factors and seasonal patterns. BMC Infect Dis 7, 107. https://doi.org/10.1186/1471-2334-
1115 7-107
1116 Huson, D.H., Beier, S., Flade, I., Górska, A., El-Hadidi, M., Mitra, S., Ruscheweyh, H.-J., Tappu, R., 2016.
1117 MEGAN Community Edition - Interactive Exploration and Analysis of Large-Scale Microbiome
1118 Sequencing Data. PLOS Computational Biology 12, e1004957.
1119 https://doi.org/10.1371/journal.pcbi.1004957
1120 Jalan, R., Pavesi, M., Saliba, F., Amorós, A., Fernandez, J., Holland-Fischer, P., Sawhney, R., Mookerjee,
1121 R., Caraceni, P., Moreau, R., Ginès, P., Durand, F., Angeli, P., Alessandria, C., Laleman, W.,
1122 Trebicka, J., Samuel, D., Zeuzem, S., Gustot, T., Gerbes, A.L., Wendon, J., Bernardi, M., Arroyo,
1123 V., CANONIC Study Investigators; EASL-CLIF Consortium, 2015. The CLIF Consortium Acute
1124 Decompensation score (CLIF-C ADs) for prognosis of hospitalised cirrhotic patients without
1125 acute-on-chronic liver failure. J Hepatol 62, 831–840.
1126 https://doi.org/10.1016/j.jhep.2014.11.012
1127 Jin, M., Kalainy, S., Baskota, N., Chiang, D., Deehan, E.C., McDougall, C., Tandon, P., Martínez, I.,
1128 Cervera, C., Walter, J., Abraldes, J.G., 2019. Faecal microbiota from patients with cirrhosis has
1129 a low capacity to ferment non-digestible carbohydrates into short-chain fatty acids. Liver Int
1130 39, 1437–1447. https://doi.org/10.1111/liv.14106
1131 Jordan, J.A., Durso, M.B., 2005. Real-time polymerase chain reaction for detecting bacterial DNA
1132 directly from blood of neonates being evaluated for sepsis. J Mol Diagn 7, 575–581.
1133 https://doi.org/10.1016/S1525-1578(10)60590-9
1134 Kakiyama, G., Muto, A., Takei, H., Nittono, H., Murai, T., Kurosawa, T., Hofmann, A.F., Pandak, W.M.,
1135 Bajaj, J.S., 2014. A simple and accurate HPLC method for fecal bile acid profile in healthy and
1136 cirrhotic subjects: validation by GC-MS and LC-MS. J Lipid Res 55, 978–990.
1137 https://doi.org/10.1194/jlr.D047506
1138 Kakiyama, G., Pandak, W.M., Gillevet, P.M., Hylemon, P.B., Heuman, D.M., Daita, K., Takei, H., Muto,
1139 A., Nittono, H., Ridlon, J.M., White, M.B., Noble, N.A., Monteith, P., Fuchs, M., Thacker, L.R.,
1140 Sikaroodi, M., Bajaj, J.S., 2013. Modulation of the fecal bile acid profile by gut microbiota in
1141 cirrhosis. J Hepatol 58, 949–955. https://doi.org/10.1016/j.jhep.2013.01.003
1142 Katoonizadeh, A., Laleman, W., Verslype, C., Wilmer, A., Maleux, G., Roskams, T., Nevens, F., 2010.
1143 Early features of acute-on-chronic alcoholic liver failure: a prospective cohort study. Gut 59,
1144 1561–1569. https://doi.org/10.1136/gut.2009.189639
1145 Kim, W.R., Biggins, S.W., Kremers, W.K., Wiesner, R.H., Kamath, P.S., Benson, J.T., Edwards, E.,
1146 Therneau, T.M., 2008. Hyponatremia and mortality among patients on the liver-transplant
1147 waiting list. N Engl J Med 359, 1018–1026. https://doi.org/10.1056/NEJMoa0801209
1148 Kiu, R., Brown, J., Bedwell, H., Leclaire, C., Caim, S., Pickard, D., Dougan, G., Dixon, R.A., Hall, L.J.,
1149 2019. Genomic analysis on broiler-associated Clostridium perfringens strains and exploratory

1150 caecal microbiome investigation reveals key factors linked to poultry necrotic enteritis.
1151 Animal Microbiome 1, 12. https://doi.org/10.1186/s42523-019-0015-1
1152 Le Guennec, A., Tayyari, F., Edison, A.S., 2017. Alternatives to Nuclear Overhauser Enhancement
1153 Spectroscopy Presat and Carr-Purcell-Meiboom-Gill Presat for NMR-Based Metabolomics.
1154 Anal Chem 89, 8582–8588. https://doi.org/10.1021/acs.analchem.7b02354
1155 Lee, S., Arefaine, B., Begum, N., Stamouli, M., Witherden, E., Mohamad, M., Harzandi, A., Zamalloa,
1156 A., Cai, H., Williams, R., Curtis, M., Edwards, L.A., Chokshi, S., Mardinoglu, A., Proctor, G.,
1157 Moyes, D., McPhail, M.J., Shawcross, D.L., Uhlen, M., Shoaie, S., Patel, V.C., 2024a. Oral-gut
1158 microbiome interactions in advanced cirrhosis: characterisation of pathogenic enterotypes
1159 and salivatypes, virulence factors and antimicrobial. J Hepatol S0168-8278(24)02635–7.
1160 https://doi.org/10.1016/j.jhep.2024.09.046
1161 Lee, S., Arefaine, B., Begum, N., Stamouli, M., Witherden, E., Mohamad, M., Harzandi, A., Zamalloa,
1162 A., Cai, H., Williams, R., Curtis, M.A., Edwards, L.A., Chokshi, S., Mardinoglu, A., Proctor, G.,
1163 Moyes, D.L., McPhail, M.J., Shawcross, D.L., Uhlen, M., Shoaie, S., Patel, V.C., 2024b. Oral-gut
1164 microbiome interactions in advanced cirrhosis: characterisation of pathogenic enterotypes
1165 and salivatypes, virulence factors and antimicrobial resistance. Journal of Hepatology 0.
1166 https://doi.org/10.1016/j.jhep.2024.09.046
1167 Lees, H.J., Swann, J.R., Wilson, I.D., Nicholson, J.K., Holmes, E., 2013. Hippurate: the natural history
1168 of a mammalian-microbial cometabolite. J Proteome Res 12, 1527–1546.
1169 https://doi.org/10.1021/pr300900b
1170 Letunic, I., Bork, P., 2019. Interactive Tree Of Life (iTOL) v4: recent updates and new developments.
1171 Nucleic Acids Research 47, W256–W259. https://doi.org/10.1093/nar/gkz239
1172 Liu, B., Zheng, D., Jin, Q., Chen, L., Yang, J., 2019. VFDB 2019: a comparative pathogenomic platform
1173 with an interactive web interface. Nucleic Acids Research 47, D687–D692.
1174 https://doi.org/10.1093/nar/gky1080
1175 Love, M.I., Huber, W., Anders, S., 2014. Moderated estimation of fold change and dispersion for RNA-
1176 seq data with DESeq2. Genome Biol 15, 550. https://doi.org/10.1186/s13059-014-0550-8
1177 Mallick, H., Rahnavard, A., McIver, L.J., Ma, S., Zhang, Y., Nguyen, L.H., Tickle, T.L., Weingart, G., Ren,
1178 B., Schwager, E.H., Chatterjee, S., Thompson, K.N., Wilkinson, J.E., Subramanian, A., Lu, Y.,
1179 Waldron, L., Paulson, J.N., Franzosa, E.A., Bravo, H.C., Huttenhower, C., 2021. Multivariable
1180 association discovery in population-scale meta-omics studies. PLOS Computational Biology
1181 17, e1009442. https://doi.org/10.1371/journal.pcbi.1009442
1182 Martinez Arbizu, P., 2020. pairwiseAdonis: Pairwise multilevel comparison using adonis.
1183 Moreau, R., Jalan, R., Gines, P., Pavesi, M., Angeli, P., Cordoba, J., Durand, F., Gustot, T., Saliba, F.,
1184 Domenicali, M., Gerbes, A., Wendon, J., Alessandria, C., Laleman, W., Zeuzem, S., Trebicka, J.,
1185 Bernardi, M., Arroyo, V., CANONIC Study Investigators of the EASL–CLIF Consortium, 2013.
1186 Acute-on-chronic liver failure is a distinct syndrome that develops in patients with acute
1187 decompensation of cirrhosis. Gastroenterology 144, 1426–1437, 1437.e1–9.
1188 https://doi.org/10.1053/j.gastro.2013.02.042
1189 Moubareck, C., Gavini, F., Vaugien, L., Butel, M.J., Doucet-Populaire, F., 2005. Antimicrobial
1190 susceptibility of bifidobacteria. J Antimicrob Chemother 55, 38–44.
1191 https://doi.org/10.1093/jac/dkh495
1192 Mouzaki, M., Wang, A.Y., Bandsma, R., Comelli, E.M., Arendt, B.M., Zhang, L., Fung, S., Fischer, S.E.,
1193 McGilvray, I.G., Allard, J.P., 2016. Bile Acids and Dysbiosis in Non-Alcoholic Fatty Liver Disease.
1194 PLoS One 11, e0151829. https://doi.org/10.1371/journal.pone.0151829

1195 Nallapareddy, S.R., Singh, K.V., Okhuysen, P.C., Murray, B.E., 2008. A functional collagen adhesin
1196 gene, acm, in clinical isolates of Enterococcus faecium correlates with the recent success of
1197 this emerging nosocomial pathogen. Infect Immun 76, 4110–4119.
1198 https://doi.org/10.1128/IAI.00375-08
1199 Odenwald, M.A., Lin, H., Lehmann, C., Dylla, N.P., Cole, C.G., Mostad, J.D., Pappas, T.E., Ramaswamy,
1200 R., Moran, A., Hutchison, A.L., Stutz, M.R., Dela Cruz, M., Adler, E., Boissiere, J., Khalid, M.,
1201 Cantoral, J., Haro, F., Oliveira, R.A., Waligurski, E., Cotter, T.G., Light, S.H., Beavis, K.G.,
1202 Sundararajan, A., Sidebottom, A.M., Reddy, K.G., Paul, S., Pillai, A., Te, H.S., Rinella, M.E.,
1203 Charlton, M.R., Pamer, E.G., Aronsohn, A.I., 2023. Bifidobacteria metabolize lactulose to
1204 optimize gut metabolites and prevent systemic infection in patients with liver disease. Nat
1205 Microbiol 1–17. https://doi.org/10.1038/s41564-023-01493-w
1206 Oksanen, F., 2017. Vegan: Community Ecology Package.
1207 Organ, C.L., Li, Z., Sharp, T.E., Polhemus, D.J., Gupta, N., Goodchild, T.T., Tang, W.H.W., Hazen, S.L.,
1208 Lefer, D.J., 2020. Nonlethal Inhibition of Gut Microbial Trimethylamine N-oxide Production
1209 Improves Cardiac Function and Remodeling in a Murine Model of Heart Failure. Journal of the
1210 American Heart Association 9, e016223. https://doi.org/10.1161/JAHA.119.016223
1211 Page, A.J., Taylor, B., Delaney, A.J., Soares, J., Seemann, T., Keane, J.A., Harris, S.R., 2016. SNP-sites:
1212 rapid efficient extraction of SNPs from multi-FASTA alignments. Microb Genom 2, e000056.
1213 https://doi.org/10.1099/mgen.0.000056
1214 Pallister, T., Jackson, M.A., Martin, T.C., Zierer, J., Jennings, A., Mohney, R.P., MacGregor, A., Steves,
1215 C.J., Cassidy, A., Spector, T.D., Menni, C., 2017. Hippurate as a metabolomic marker of gut
1216 microbiome diversity: Modulation by diet and relationship to metabolic syndrome. Sci Rep 7,
1217 13670. https://doi.org/10.1038/s41598-017-13722-4
1218 Peterson, R.A., 2021. Finding Optimal Normalizing Transformations via bestNormalize. The R Journal
1219 13, 310–329.
1220 Peterson, R.A., Cavanaugh, J.E., 2020. Ordered quantile normalization: a semiparametric
1221 transformation built for the cross-validation era. Journal of Applied Statistics 47, 2312–2327.
1222 https://doi.org/10.1080/02664763.2019.1630372
1223 Piano, S., Singh, V., Caraceni, P., Maiwall, R., Alessandria, C., Fernandez, J., Soares, E.C., Kim, D.J., Kim,
1224 S.E., Marino, M., Vorobioff, J., Barea, R. de C.R., Merli, M., Elkrief, L., Vargas, V., Krag, A., Singh,
1225 S.P., Lesmana, L.A., Toledo, C., Marciano, S., Verhelst, X., Wong, F., Intagliata, N., Rabinowich,
1226 L., Colombato, L., Kim, S.G., Gerbes, A., Durand, F., Roblero, J.P., Bhamidimarri, K.R., Boyer,
1227 T.D., Maevskaya, M., Fassio, E., Kim, H.S., Hwang, J.S., Gines, P., Gadano, A., Sarin, S.K., Angeli,
1228 P., International Club of Ascites Global Study Group, 2019. Epidemiology and Effects of
1229 Bacterial Infections in Patients With Cirrhosis Worldwide. Gastroenterology 156, 1368-
1230 1380.e10. https://doi.org/10.1053/j.gastro.2018.12.005
1231 Price, M.N., Dehal, P.S., Arkin, A.P., 2009. FastTree: Computing Large Minimum Evolution Trees with
1232 Profiles instead of a Distance Matrix. Molecular Biology and Evolution 26, 1641–1650.
1233 https://doi.org/10.1093/molbev/msp077
1234 Pugh, R.N., Murray-Lyon, I.M., Dawson, J.L., Pietroni, M.C., Williams, R., 1973. Transection of the
1235 oesophagus for bleeding oesophageal varices. Br J Surg 60, 646–649.
1236 https://doi.org/10.1002/bjs.1800600817
1237 Quast, C., Pruesse, E., Yilmaz, P., Gerken, J., Schweer, T., Yarza, P., Peplies, J., Glöckner, F.O., 2013.
1238 The SILVA ribosomal RNA gene database project: improved data processing and web-based
1239 tools. Nucleic Acids Research 41, D590–D596. https://doi.org/10.1093/nar/gks1219

1240 Ridlon, J.M., Alves, J.M., Hylemon, P.B., Bajaj, J.S., 2013. Cirrhosis, bile acids and gut microbiota:
1241 unraveling a complex relationship. Gut Microbes 4, 382–387.
1242 https://doi.org/10.4161/gmic.25723
1243 Riva, A., Gray, E.H., Azarian, S., Zamalloa, A., McPhail, M.J.W., Vincent, R.P., Williams, R., Chokshi, S.,
1244 Patel, V.C., Edwards, L.A., 2020. Faecal cytokine profiling as a marker of intestinal
1245 inflammation in acutely decompensated cirrhosis. JHEP Rep 2, 100151.
1246 https://doi.org/10.1016/j.jhepr.2020.100151
1247 Seishima, J., Iida, N., Kitamura, K., Yutani, M., Wang, Z., Seki, A., Yamashita, Taro, Sakai, Y., Honda,
1248 M., Yamashita, Tatsuya, Kagaya, T., Shirota, Y., Fujinaga, Y., Mizukoshi, E., Kaneko, S., 2019.
1249 Gut-derived Enterococcus faecium from ulcerative colitis patients promotes colitis in a
1250 genetically susceptible mouse host. Genome Biol 20, 252. https://doi.org/10.1186/s13059-
1251 019-1879-9
1252 Shah, N.J., Mousa, O.Y., Syed, K., John, S., 2024. Acute on Chronic Liver Failure, in: StatPearls.
1253 StatPearls Publishing, Treasure Island (FL).
1254 Slanetz, L.W., Bartley, C.H., 1957. NUMBERS OF ENTEROCOCCI IN WATER, SEWAGE, AND FECES
1255 DETERMINED BY THE MEMBRANE FILTER TECHNIQUE WITH AN IMPROVED MEDIUM1. J
1256 Bacteriol 74, 591–595.
1257 Solé, C., Guilly, S., Da Silva, K., Llopis, M., Le-Chatelier, E., Huelin, P., Carol, M., Moreira, R., Fabrellas,
1258 N., De Prada, G., Napoleone, L., Graupera, I., Pose, E., Juanola, A., Borruel, N., Berland, M.,
1259 Toapanta, D., Casellas, F., Guarner, F., Doré, J., Solà, E., Ehrlich, S.D., Ginès, P., 2021.
1260 Alterations in Gut Microbiome in Cirrhosis as Assessed by Quantitative Metagenomics:
1261 Relationship With Acute-on-Chronic Liver Failure and Prognosis. Gastroenterology 160, 206-
1262 218.e13. https://doi.org/10.1053/j.gastro.2020.08.054
1263 Tagliacozzi, D., Mozzi, A.F., Casetta, B., Bertucci, P., Bernardini, S., Di Ilio, C., Urbani, A., Federici, G.,
1264 2003. Quantitative analysis of bile acids in human plasma by liquid chromatography-
1265 electrospray tandem mass spectrometry: a simple and rapid one-step method. Clin Chem Lab
1266 Med 41, 1633–1641. https://doi.org/10.1515/CCLM.2003.247
1267 Tilg, H., Adolph, T.E., Trauner, M., 2022. Gut-liver axis: Pathophysiological concepts and clinical
1268 implications. Cell Metab 34, 1700–1718. https://doi.org/10.1016/j.cmet.2022.09.017
1269 Toledo, C., Salmerón, J.M., Rimola, A., Navasa, M., Arroyo, V., Llach, J., Ginès, A., Ginès, P., Rodés, J.,
1270 1993. Spontaneous bacterial peritonitis in cirrhosis: predictive factors of infection resolution
1271 and survival in patients treated with cefotaxime. Hepatology 17, 251–257.
1272 Tonkin-Hill, G., MacAlasdair, N., Ruis, C., Weimann, A., Horesh, G., Lees, J.A., Gladstone, R.A., Lo, S.,
1273 Beaudoin, C., Floto, R.A., Frost, S.D.W., Corander, J., Bentley, S.D., Parkhill, J., 2020. Producing
1274 polished prokaryotic pangenomes with the Panaroo pipeline. Genome Biology 21, 180.
1275 https://doi.org/10.1186/s13059-020-02090-4
1276 Tranah, T.H., Edwards, L.A., Schnabl, B., Shawcross, D.L., 2021. Targeting the gut-liver-immune axis
1277 to treat cirrhosis. Gut 70, 982–994. https://doi.org/10.1136/gutjnl-2020-320786
1278 Trebicka, J., Fernandez, J., Papp, M., Caraceni, P., Laleman, W., Gambino, C., Giovo, I., Uschner, F.E.,
1279 Jansen, C., Jimenez, C., Mookerjee, R., Gustot, T., Albillos, A., Bañares, R., Jarcuska, P., Steib,
1280 C., Reiberger, T., Acevedo, J., Gatti, P., Shawcross, D.L., Zeuzem, S., Zipprich, A., Piano, S., Berg,
1281 T., Bruns, T., Danielsen, K.V., Coenraad, M., Merli, M., Stauber, R., Zoller, H., Ramos, J.P., Solé,
1282 C., Soriano, G., de Gottardi, A., Gronbaek, H., Saliba, F., Trautwein, C., Kani, H.T., Francque, S.,
1283 Ryder, S., Nahon, P., Romero-Gomez, M., Van Vlierberghe, H., Francoz, C., Manns, M., Garcia-
1284 Lopez, E., Tufoni, M., Amoros, A., Pavesi, M., Sanchez, C., Praktiknjo, M., Curto, A., Pitarch, C.,

1285 Putignano, A., Moreno, E., Bernal, W., Aguilar, F., Clària, J., Ponzo, P., Vitalis, Z., Zaccherini, G.,
1286 Balogh, B., Gerbes, A., Vargas, V., Alessandria, C., Bernardi, M., Ginès, P., Moreau, R., Angeli,
1287 P., Jalan, R., Arroyo, V., PREDICT STUDY group of the EASL-CLIF CONSORTIUM, 2021. PREDICT
1288 identifies precipitating events associated with the clinical course of acutely decompensated
1289 cirrhosis. J Hepatol 74, 1097–1108. https://doi.org/10.1016/j.jhep.2020.11.019
1290 Trovato, F.M., Zia, R., Napoli, S., Wolfer, K., Huang, X., Morgan, P.E., Husbyn, H., Elgosbi, M.,
1291 Lucangeli, M., Miquel, R., Wilson, I., Heaton, N.D., Heneghan, M.A., Auzinger, G., Antoniades,
1292 C.G., Wendon, J.A., Patel, V.C., Coen, M., Triantafyllou, E., McPhail, M.J., 2021. Dysregulation
1293 of the Lysophosphatidylcholine/Autotaxin/Lysophosphatidic Acid Axis in Acute-on-Chronic
1294 Liver Failure Is Associated With Mortality and Systemic Inflammation by Lysophosphatidic
1295 Acid-Dependent Monocyte Activation. Hepatology 74, 907–925.
1296 https://doi.org/10.1002/hep.31738
1297 van den Berg, E.H., Flores-Guerrero, J.L., Garcia, E., Connelly, M.A., de Meijer, V.E., TransplantLines
1298 Investigators, Bakker, S.J.L., Blokzijl, H., Dullaart, R.P.F., 2023. High plasma levels of betaine,
1299 a trimethylamine N-Oxide-related metabolite, are associated with the severity of cirrhosis.
1300 Liver Int 43, 424–433. https://doi.org/10.1111/liv.15310
1301 Vergis, N., Atkinson, S.R., Knapp, S., Maurice, J., Allison, M., Austin, A., Forrest, E.H., Masson, S.,
1302 McCune, A., Patch, D., Richardson, P., Gleeson, D., Ryder, S.D., Wright, M., Thursz, M.R., 2017.
1303 In Patients With Severe Alcoholic Hepatitis, Prednisolone Increases Susceptibility to Infection
1304 and Infection-Related Mortality, and Is Associated With High Circulating Levels of Bacterial
1305 DNA. Gastroenterology 152, 1068-1077.e4. https://doi.org/10.1053/j.gastro.2016.12.019
1306 Vital, M., Rud, T., Rath, S., Pieper, D.H., Schlüter, D., 2019. Diversity of Bacteria Exhibiting Bile Acid-
1307 inducible 7α-dehydroxylation Genes in the Human Gut. Comput Struct Biotechnol J 17, 1016–
1308 1019. https://doi.org/10.1016/j.csbj.2019.07.012
1309 Walker, B.J., Abeel, T., Shea, T., Priest, M., Abouelliel, A., Sakthikumar, S., Cuomo, C.A., Zeng, Q.,
1310 Wortman, J., Young, S.K., Earl, A.M., 2014. Pilon: An Integrated Tool for Comprehensive
1311 Microbial Variant Detection and Genome Assembly Improvement. PLOS ONE 9, e112963.
1312 https://doi.org/10.1371/journal.pone.0112963
1313 Wang, Q., Chen, C., Zuo, S., Cao, K., Li, H., 2023. Integrative analysis of the gut microbiota and faecal
1314 and serum short-chain fatty acids and tryptophan metabolites in patients with cirrhosis and
1315 hepatic encephalopathy. J Transl Med 21, 395. https://doi.org/10.1186/s12967-023-04262-9
1316 Wick, R.R., Judd, L.M., Gorrie, C.L., Holt, K.E., 2017. Unicycler: Resolving bacterial genome assemblies
1317 from short and long sequencing reads. PLOS Computational Biology 13, e1005595.
1318 https://doi.org/10.1371/journal.pcbi.1005595
1319 Williams, H.R.T., Cox, I.J., Walker, D.G., Cobbold, J.F.L., Taylor-Robinson, S.D., Marshall, S.E., Orchard,
1320 T.R., 2010. Differences in gut microbial metabolism are responsible for reduced hippurate
1321 synthesis in Crohn's disease. BMC Gastroenterol 10, 108. https://doi.org/10.1186/1471-
1322 230X-10-108
1323 Wong, F., Piano, S., Singh, V., Bartoletti, M., Maiwall, R., Alessandria, C., Fernandez, J., Soares, E.C.,
1324 Kim, D.J., Kim, S.E., Marino, M., Vorobioff, J., Barea, R. de C.R., Merli, M., Elkrief, L., Vargas,
1325 V., Krag, A., Singh, S.P., Lesmana, L.A., Toledo, C., Marciano, S., Verhelst, X., Intagliata, N.,
1326 Rabinowich, L., Colombato, L., Kim, S.G., Gerbes, A., Durand, F., Roblero, J.P., Bruns, T., Yoon,
1327 E.L., Girala, M., Pyrsopoulos, N.T., Kim, T.H., Yim, S.Y., Juanola, A., Gadano, A., Angeli, P.,
1328 International Club of Ascites Global Study Group, 2021. Clinical features and evolution of

1329 bacterial infection-related acute-on-chronic liver failure. J Hepatol 74, 330–339.
1330 https://doi.org/10.1016/j.jhep.2020.07.046
1331 Y, Furusawa, Y, O., S, F., Ta, E., G, N., D, T., Y, N., C, U., K, K., T, K., M, Takahashi, Nn, F., S, M., E, M., S,
1332 Hino, K, A., S, O., Y, Fujimura, T, L., Jm, C., Dl, T., M, Tomita, S, Hori, O, O., T, M., H, K., J, K., K,
1333 Honda, K, Hase, H, O., 2013. Commensal microbe-derived butyrate induces the differentiation
1334 of colonic regulatory T cells. Nature 504. https://doi.org/10.1038/nature12721
1335 Zapun, A., Contreras-Martel, C., Vernet, T., 2008. Penicillin-binding proteins and beta-lactam
1336 resistance. FEMS microbiology reviews 32. https://doi.org/10.1111/j.1574-
1337 6976.2007.00095.x
1338 Zhang, J., Kobert, K., Flouri, T., Stamatakis, A., 2014. PEAR: a fast and accurate Illumina Paired-End
1339 reAd mergeR. Bioinformatics 30, 614–620. https://doi.org/10.1093/bioinformatics/btt593
1340 Zhang, X., Bierschenk, D., Top, J., Anastasiou, I., Bonten, M.J., Willems, R.J., van Schaik, W., 2013.
1341 Functional genomic analysis of bile salt resistance in Enterococcus faecium. BMC Genomics
1342 14, 299. https://doi.org/10.1186/1471-2164-14-299
1343 Zimmermann, P., Curtis, N., 2019. The effect of antibiotics on the composition of the intestinal
1344 microbiota - a systematic review. The Journal of infection 79.
1345 https://doi.org/10.1016/j.jinf.2019.10.008

1346

1347

1348 **Table 1**: Summary of clinical characteristics of patient and healthy participant study groups (all values given as median [IQR])

Parameters			HC (n=40)	SC (n=15)	DC (n=81)	ACLF (n=57)	P value
General	Age (years)		36 (32-41)	59 (54-69)	55 (49-61)	49 (42-59)	<0.0001
	Male gender (n (%))		20 (50%)	11 (73.3%)	52 (64.2%)	36 (63.2%)	0.3287
	BMI (kg/m^2)		N/A	27.2 (23.5-32.6)	27.4 (24.0-30.5)	22.7 (20.8-23.2)	<0.0001
Aetiology of cirrhosis	Alcohol-related liver disease (n (%))		N/A	9 (60%)	57 (70.4%)	33 (57.9%)	0.2950
	Drinking/ Abstinent	Alcohol actively drinking (n (%))	N/A	0	12 (21%)	19 (57.6%)	0.0002
		Alcohol abstinent (n (%))	N/A	9 (100%)	45 (79%)	14 (42.4%)	
	Metabolic- dysfunction associated steatotic liver disease (MASLD) (n (%))		N/A	3 (20%)	7 (8.6%)	6 (10.5%)	0.4181
	Cholestatic/autoimmune (n (%)): Primary biliary cholangitis (PBC), primary sclerosing cholangitis (PSC), Alagille syndrome, biliary atresia, and autoimmune hepatitis (AIH)		N/A	1 (6.7%)	6 (7.4%)	11 (19.3%)	0.0832
	Metabolic (number (%)):		N/A	1 (6.7%)	5 (6.2%)	3 (5.3%)	0.9663

1

	Wilson's disease, haemochromatosis and alpha-1-antitrypsin (A1AT) deficiency						
	Other (n (%)): 'Cryptogenic', treated viral hepatitis, chronic veno-occlusive related-cirrhosis (Bud Chiari), chronic porto-mesenteric venous insufficiency cirrhosis, and drug induced		N/A	1 (6.7%)	6 (7.4%)	4 (7%)	0.9928
Clinical features at enrolment	Temperature (°C)		N/A	36.5 (36.3-37.2)	36.7 (36.4-37.0)	36.5 (36.1-37.1)	0.2121
	Ascites present (n (%))		N/A	5 (33.3%)	58 (71.6%)	55 (96.5%)	<0.0001
	Ascites grade (n (%))	Small	N/A	5 (100%)	25 (43.1%)	35 (63.6%)	0.0107
		Moderate / Severe	N/A	0	33 (56.9%)	20 (36.4%)	
	Hepatic encephalopathy present (n (%))		N/A	1 (6.7%)	35 (43.2%)	49 (86%)	<0.0001
	Hepatic encephalopathy grade	1-2	N/A	1 (100%)	35 (43%)	24 (49%)	<0.0001
		3-4	N/A	0	0	25 (51%)	
	Mean arterial pressure (mmHg)		N/A	95 (87-100)	81 (76-89)	75 (70-82)	<0.0001
	Presence of bacterial infection (n (%))	Blood culture	N/A	0	2 (2.5%)	3 (5.3%)	0.4996
		Urine culture	N/A	0	5 (6.2%)	2 (3.5%)	0.5114

	Heart rate (beats per minute)	N/A	76 (65-82)	77 (60-88)	87 (78-95)	0.0010
Antibacterial therapy at enrolment (number (%))	Antibiotics – any	N/A	3 (20%)	37 (45.7%)	52 (91.2%)	<0.0001
	Antifungal – any	N/A	0	2 (2.4%)	20 (35.1%)	<0.0001
	Rifaximin	N/A	1 (6.7%)	10 (12.4%)	2 (3.5%)	0.2583
	Fluoroquinolone (Norfloxacin, Ciprofloxacin)	N/A	0	8 (9.9%)	0	0.0702
Other pharmacotherapy at enrolment (number (%))	Proton pump inhibitors (Omeprazole, Lansoprazole)	N/A	10 (66.7%)	44 (54.3%)	36 (63.2%)	0.4721
	Lactulose	N/A	2 (13.3%)	30 (37.0%)	2 (3.5%)	0.1234
	Non-selective beta-blockers (Propranolol, Carvedilol)	N/A	6 (40%)	34 (42.0%)	14 (24.6%)	0.1001
	H2 antagonist (Ranitidine)	N/A	0	3 (3.7%)	0	0.2567
Laboratory parameters	Haemoglobin (g/dl)	N/A	130 ± 25	112 ± 21	92 ± 15	<0.0001
	Leukocyte count ($x10^9$/L)	N/A	4.46 (3.96-6.11)	5.57 (4.25-7.39)	9.74 (6.54-14.57)	<0.0001
	Neutrophils ($x10^9$/L)	N/A	2.92 (2.14-3.69)	3.70 (2.37-5.29)	7.70 (4.85-12.21)	<0.0001
	Platelet count ($x10^9$/L)	N/A	111 (99-151)	106 (75-165)	86 (56-115)	0.0061

	INR	N/A	1.15 (1.10-1.29)	1.44 (1.29-1.75)	2.09 (1.69-2.93)	<0.0001
	Serum creatinine (µmol/L)	N/A	73 (66-84)	77 (57-94)	135 (87-206)	<0.0001
	Serum bilirubin (µmol/L)	N/A	20 (11-25)	41 (24-72)	209 (84-371)	<0.0001
	Albumin (g/L)	N/A	39 ± 4	33 ± 6	27 ± 7	<0.0001
	C-reactive protein (mg/L)	N/A	5.5 (2.3-11.1)	11.7 (3.4-32.9)	47.3 (23.7-70.7)	<0.0001
	Blood lactate (mmol/L)	N/A	1.4 (1.2-1.9)	1.5 (1.2-2.1)	2 (1.6-3.2)	0.0006
	Venous ammonia (µmol/L)	N/A	61 (28-88)	53 (33-72)	68 (47-107)	0.0710
Disease severity & prognostic scores	Child Pugh	N/A	6 (5-6)	8 (8-10)	12 (11-13)	<0.0001
	MELD	N/A	9 (8-11)	16 (12-23)	34 (29-39)	<0.0001
	UKELD	N/A	49 ± 3	55 ± 5	61 ± 6	<0.0001
	CLIF-C-AD	N/A	N/A	49 (43-53)	N/A	—
	CLIF-C-ACLF	N/A	N/A	N/A	54 (46-66)	—
	CLIF-OF	N/A	N/A	7 (6-8)	13 (11-15)	<0.0001
Transplant-free survival	30-day	N/A	0	72 (88.9%)	24 (42.1%)	<0.0001
	90-day	N/A	0	63 (77.8%))	14 (24.6%)	<0.0001

1349

1350 # 7. Supplementary data

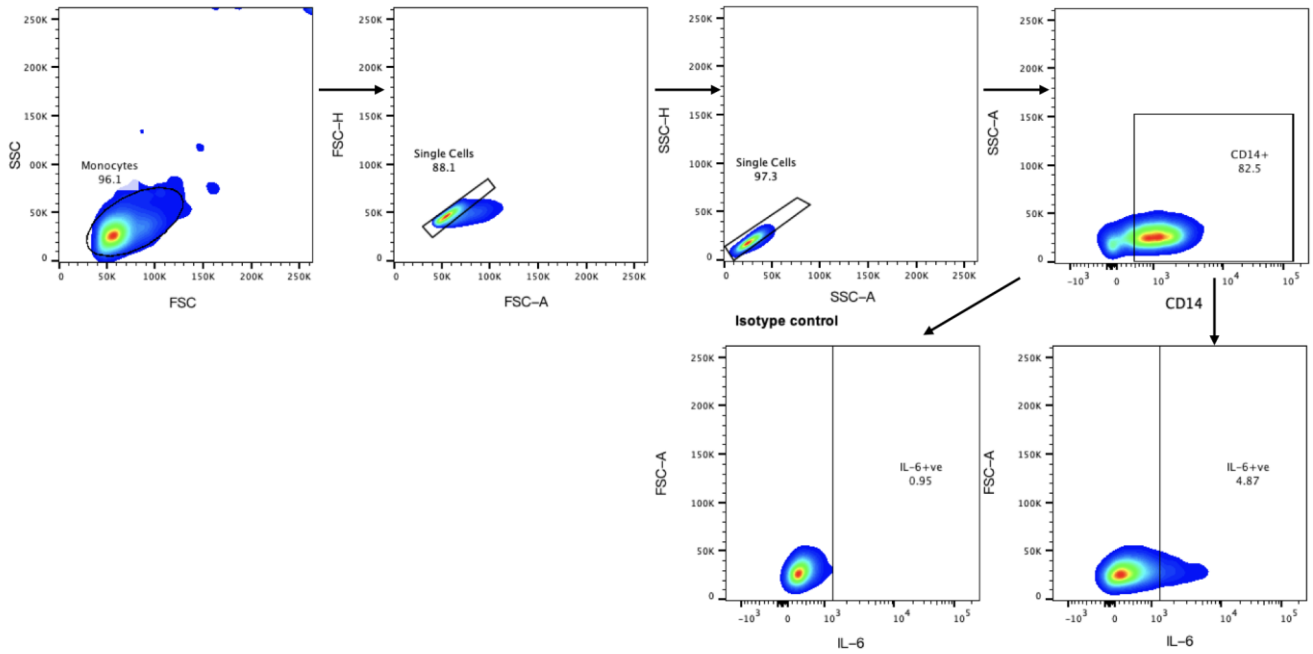

1351

1352 **Supplementary Figure 1.** Representative FACS gating strategy used to identify CD14+ monocytes in
1353 peripheral blood mononuclear cells (PBMCs) with isotype control used to determine the IL-6-
1354 producing monocytes (%) in response to LPS stimulation. Side scatter (SSC), forward scatter (FSC).

1355

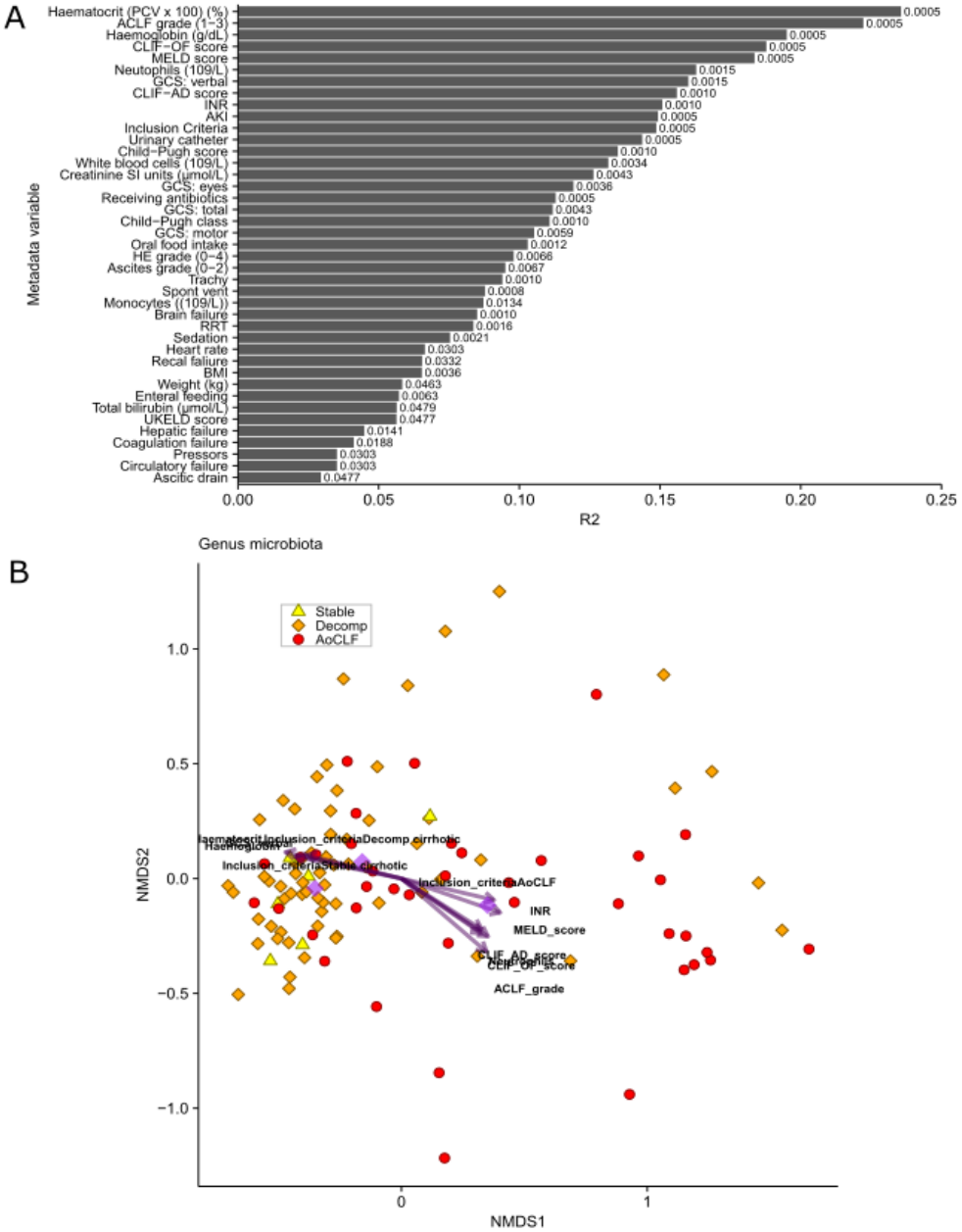

Supplementary Figure 2. Clinical metadata associated with cirrhosis patient gut microbiota composition.

(A) Results of envfit analysis showing clinical metadata variables significantly associated with microbiota composition after correction for multiple testing using False Discovery Rate. Bars show the R2 (squared correlation coefficient) of the correlation and numbers on bars show adjusted P-values. (B) NMDS ordination plot showing gut microbiota composition of individual liver patients with the ten clinical metadata variables with the highest R2 overlayed.

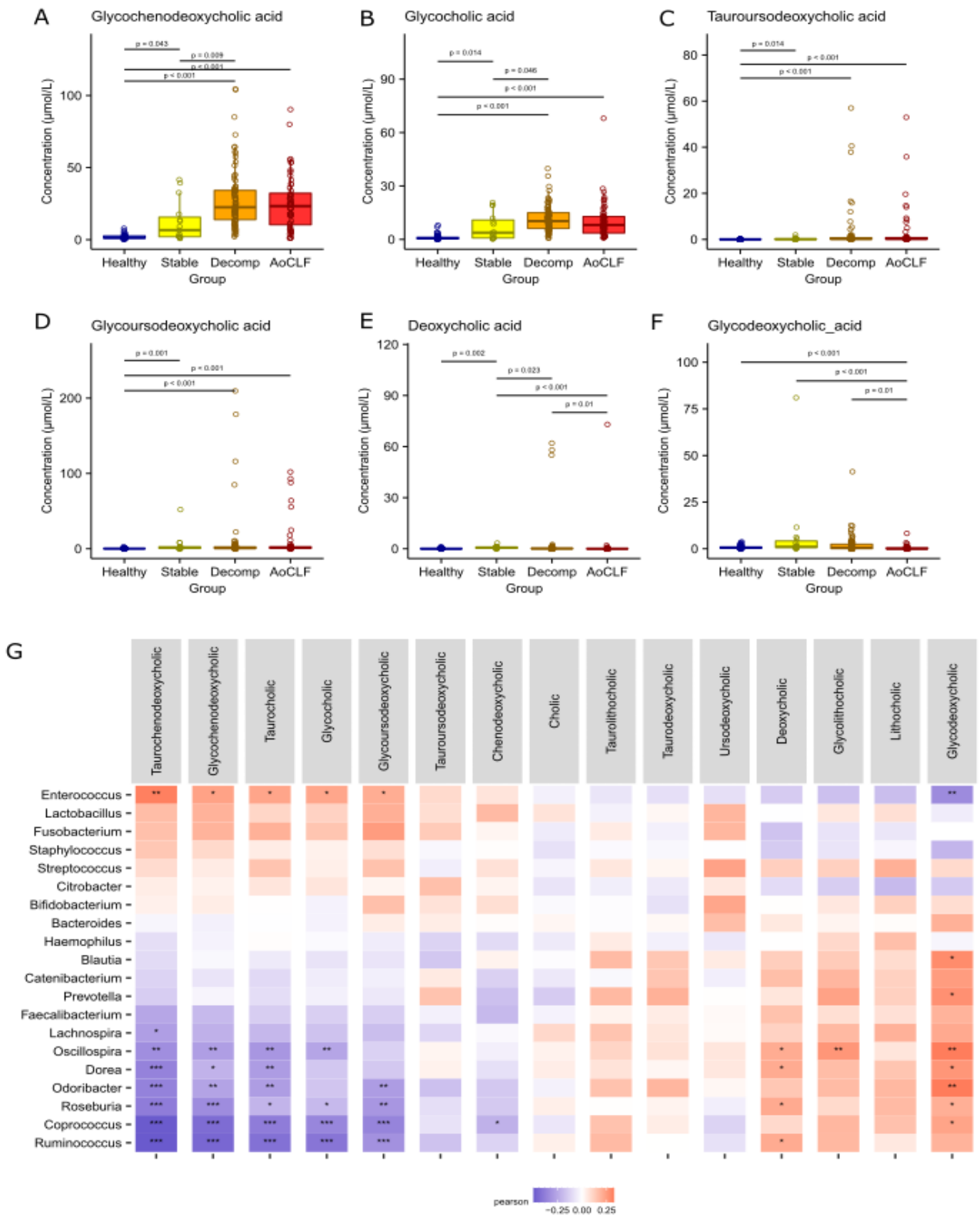

Supplementary Figure 3. Individual bile acid concentrations by cirrhosis severity and correlations between genus proportion and bile acids.

1367 (A) Glycochenodeoxycholic acid, (B) Glycocholic acid, (C) Tauroursodeoxycholic acid, (D)
1368 Glycoursodeoxycholic acid, (E) Deoxycholic acid, (F) Glycodeoxycholic acid, (F) Pearson correlations
1369 between normalised plasma bile acid concentrations and normalised genus relative abundance using
1370 a Pearson correlation. P-value: * = $p<0.05$, ** = $p<0.01$, ** = $p<0.001$. Significance corrected for
1371 multiple testing.

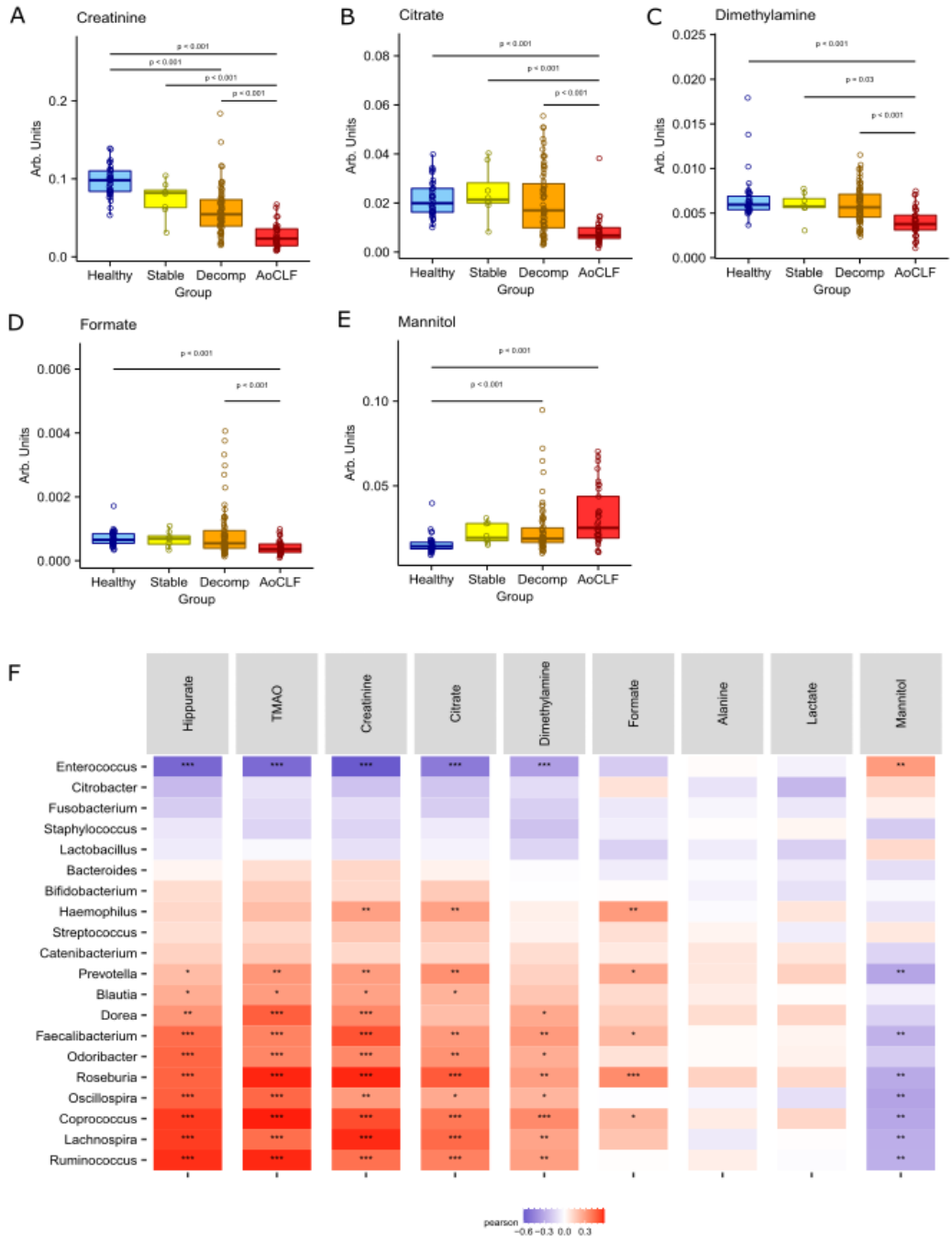

Supplementary Figure 4. Individual urinary metabolites by cirrhosis severity and correlations between genus proportion and plasma metabolites.

(A) Creatinine, (B) Citrate, (C) Dimethylamine, (D) Formate, (E) Mannitol, (F) Correlations between normalised urinary metabolites and normalised genus relative abundance using a Pearson correlation. P-value: * = p<0.05, ** = p<0.01, ** = p<0.001. Significance corrected for multiple testing.

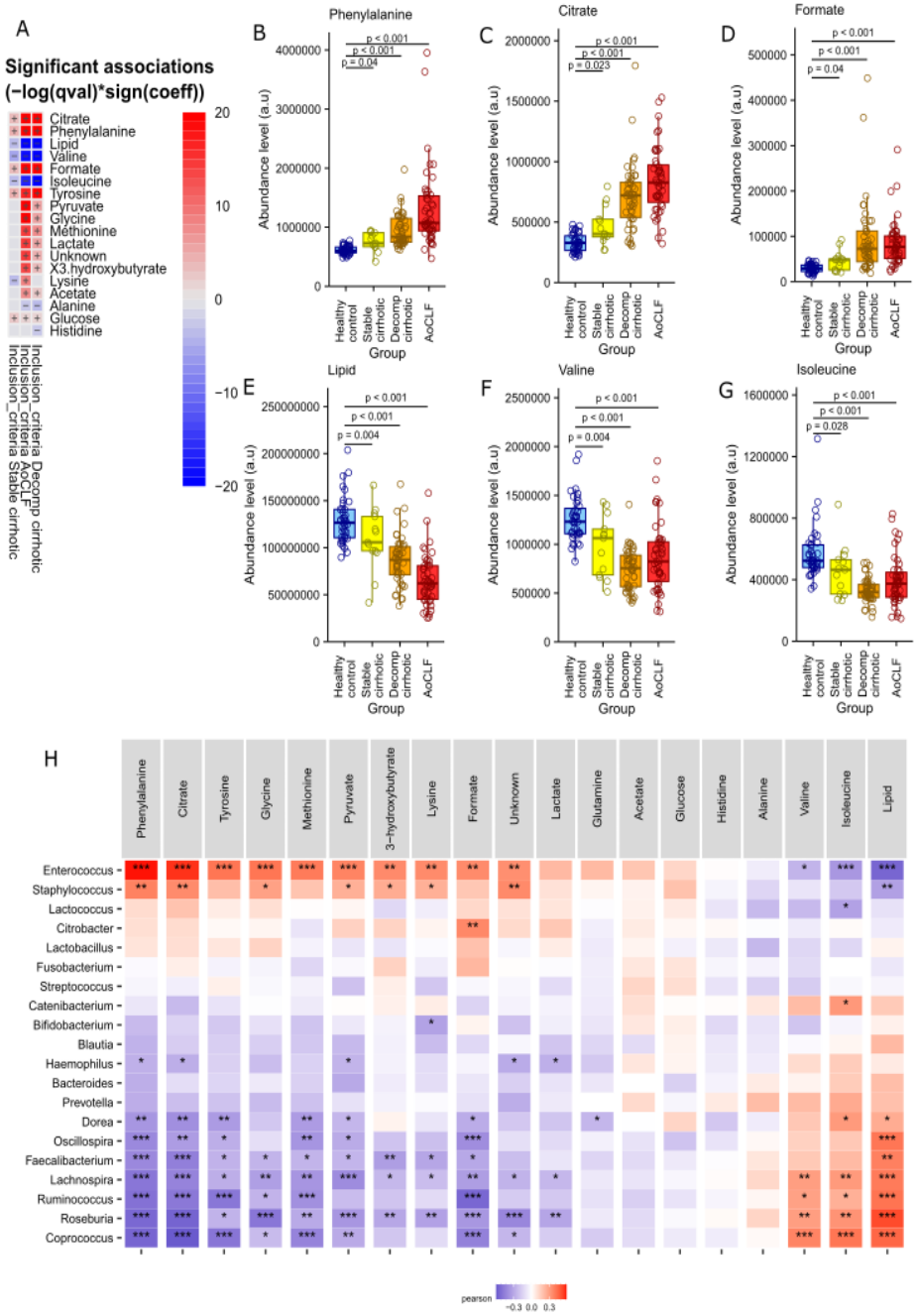

Supplementary Figure 5. Individual plasma metabolites by cirrhosis severity and correlations between genus proportion and plasma metabolites.

(A) Phenylalanine, (B) Citrate, (C) Formate, (D) Lipid, (E) Valine, (F) Isoleucine, (G) Correlations between normalised plasma metabolites and normalised genus relative abundance using a Pearson correlation. P-value: * = p<0.05, ** = p<0.01, *** = p<0.001. Significance corrected for multiple testing.

1385

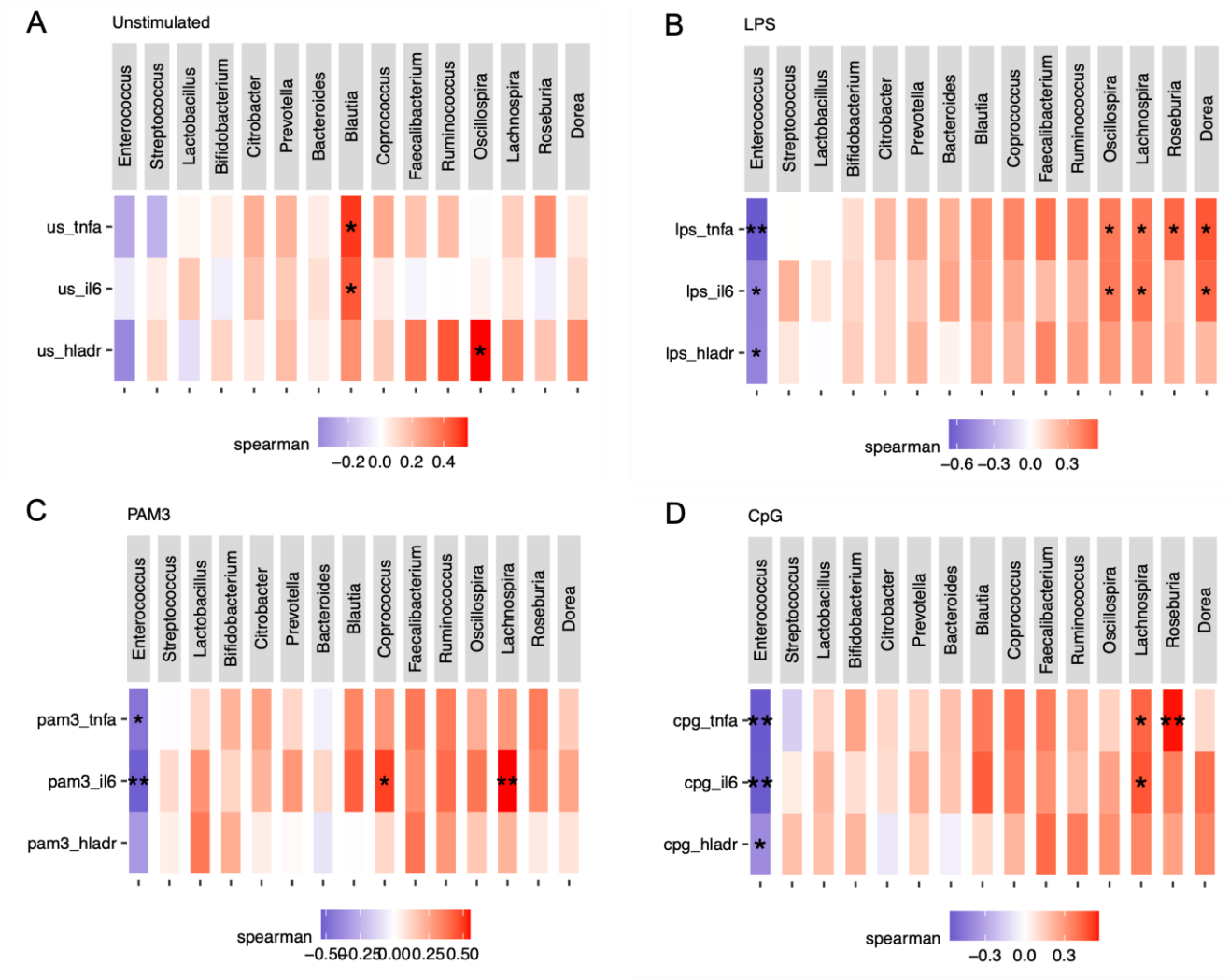

1386

1387 **Supplementary Figure 6**. Correlations between genus proportion and monocyte stimulation.

1388 Full correlations between the top 15 most abundant genera and TNF-alpha, IL-6, and HLA-DR
1389 percentage in (A) Unstimulated, (B) LPS stimulated, (C) PAM3 stimulated, and (D) CpG simulated
1390 monocytes. Correlations between normalised plasma metabolites and normalised genus relative
1391 abundance using a Pearson correlation. P-value: * = $p<0.05$, ** = $p<0.01$. Significance corrected for
1392 multiple testing.

1393

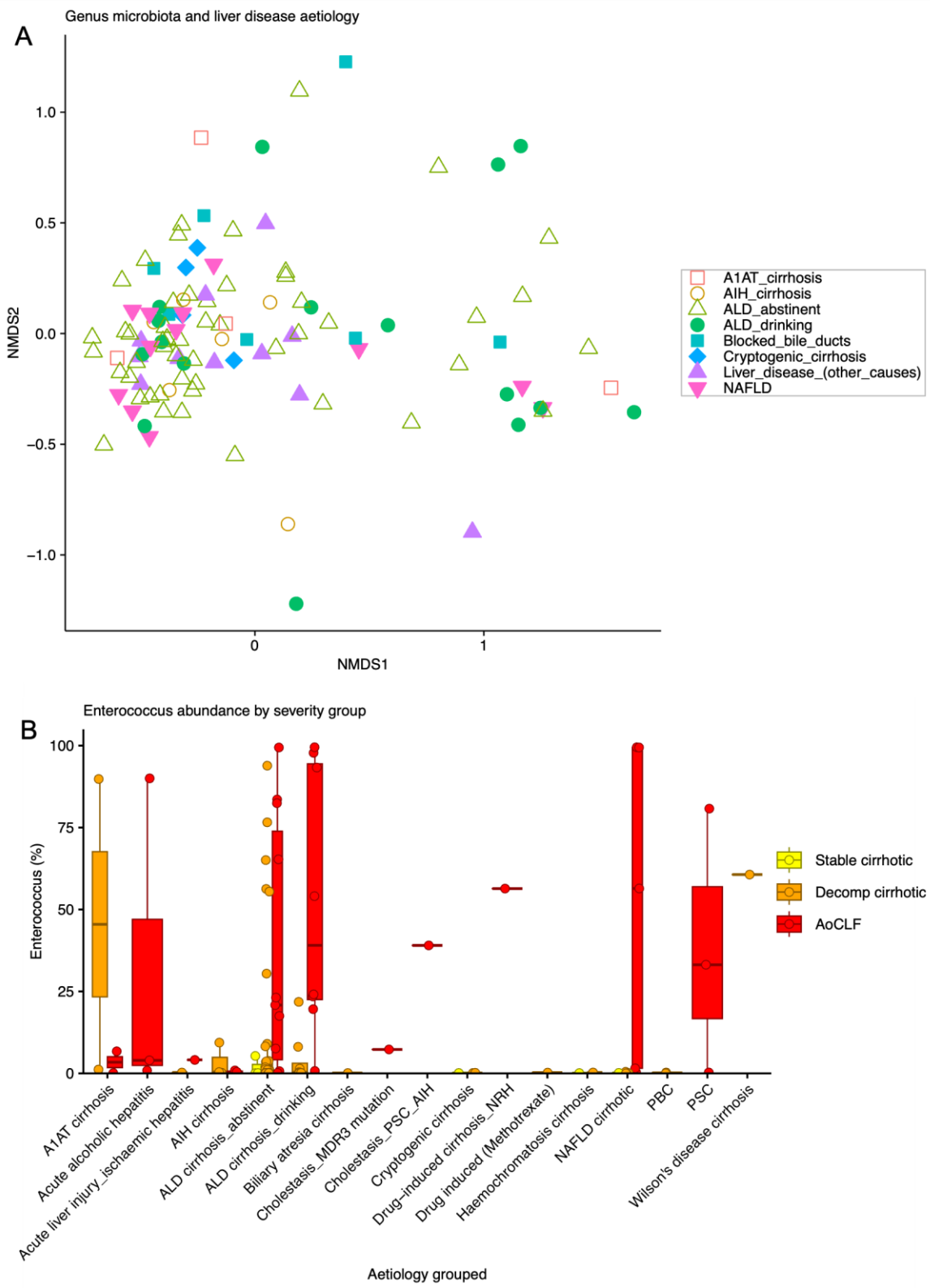

1394

1395 **Supplementary Figure 7**. Aetiology associations with overall microbiota composition and

1396 *Enterococcus* abundance.

1397 (A) NMDS clustering of overall genus level faecal microbiota composition based on a Bray-Curtis
1398 matrix showing patient samples with patient aetiology condensed to eight groups for the purposes
1399 of analysis showing a lack of clustering by aetiology (PERMANOVA: P = 0.1). (B) Box plots show full
1400 patient aetiology groups with faecal *Enterococcus* abundance grouped by illness severity.